Journal of Environmental Chemical Engineering 11 (2023) 110097

Contents lists available at ScienceDirect

Journal of Environmental Chemical Engineering

journal homepage: www.elsevier.com/locate/jece

Porphyrin-silica gel hybrids as effective and selective copper(II) adsorbents from industrial wastewater

Chahrazad El Abiad [a], Smaail Radi [a,*], Mohamed El Massaoudi [a,b], Morad Lamsayah [a], Flávio Figueira [c], M. Amparo F. Faustino [d], M. Graça P.M.S. Neves [d], Nuno M.M. Moura [d,*]

[a] Mohammed First University, Faculty of Sciences, LCAE, 60000 Oujda, Morocco
[b] Higher School of Education and Training of Oujda, PO Box: 1458, Oujda 62000, Morocco
[c] CICECO, Department of Chemistry, University of Aveiro, 3810-193 Aveiro, Portugal
[d] LAQV-REQUIMTE, Department of Chemistry, University of Aveiro, 3810-193 Aveiro, Portugal

ARTICLE INFO

Editor: Luigi Rizzo

Keywords:
Hybrid materials
Porphyrin
Immobilization
Water pollution
Hazardous metal ions
Adsorption

ABSTRACT

Porphyrins are an important class of ligands with a tremendous ability to capture metal ions closely related to the rich coordination chemistry of porphyrins. Herein we use this characteristic to develop silica gel grafted derivatives for water remediation applications. Therefore, two porphyrin derivatives, one with three and the other with four mercaptopyridyl units were grafted on silica gel functionalized with 3-aminopropyltriethoxysilane. The new adsorbents **Si3PyS** and **Si4PyS** were characterized using a suitable set of techniques confirming the covalent attachment of the porphyrins to the silica surface. Additionally, microscopy and N_2 adsorption analysis confirmed the structural integrity and preservation of the mesoporous structure of **Si** during surface modification. The results show that both hybrid materials exhibit good chemical and thermal stability and an outstanding Cu^{2+} removal capability, with a chemical adsorption capacity of 176.32 mg g^{-1} and 184.16 mg g^{-1}, respectively. These materials have also been used in real water and industrial wastewater samples with minimal interference in their adsorption capabilities. Density Functional Theory calculations were performed to confirm the good performance of the hybrid materials **Si3PyS** and **Si4PyS** towards metal ions. The functionalization of silica surface with porphyrin-based ligands bearing additional binding motifs drastically improves the adsorption capability of the new hybrids towards metal ions. The presence of pyridyl units brings a meaningful advantage, since both porphyrin core and appended pyridyl groups are able of binding Cu^{2+} ions with high affinity, contributing to the enhancement of the chelating features of the adsorbents prepared when compared with other ligands supported in silica-based materials.

1. Introduction

Nowadays, the appearance of a large panoply of contaminants of emerging concern (e.g. personal care products, hormones, pharmaceutically active compounds or industrial chemicals where are included hazardous metal ions) in residual water prompted the scientific community to develop advanced treatment processes to remove them in wastewater plants [1–5]. In particular, in industrial areas, pollution by hazardous metal ions has turned out one of the major threats to the environment as well as public health, since they are not biodegradable, and consequently their accumulation in the environment can reach hazardous concentrations levels [6]. Long-term exposure to potentially toxic metals ions, such as Cu^{2+}, Pb^{2+}, Cd^{2+}, and Zn^{2+} are being associated with liver and kidney damage, reduction in hemoglobin formation, hypertension, testicular atrophy diseases or itching, lung cancer, memory or concentration problems, kidney failure, and nervous diseases [7–9].

Hazardous metal ions are released into the environment either by industrial activity or as natural deposits present in the Earth crust [10]. Industrial activities related to mining, metal fishing, plating, storage batteries and semiconductors are, among others, the major sources for the release of heavy metals into the wastewater. Advanced wastewater treatment processes are essential for removing residual pollutants that remain in wastewater after primary and biological treatment, including hazardous metal ions that microorganisms are unable to degrade. Removal of hazardous metal ions is a crucial step that must be

* Corresponding authors.
E-mail addresses: s.radi@ump.ac.ma (S. Radi), nmoura@ua.pt (N.M.M. Moura).

https://doi.org/10.1016/j.jece.2023.110097
Received 7 February 2023; Received in revised form 19 April 2023; Accepted 9 May 2023
Available online 10 May 2023

performed before water release. This is necessary to ensure the safety and cleanliness of the wastewater before it is discharged into the environment or reused for other purposes. Therefore, in recent years, the removal of hazardous metals from natural waters and wastewater is attracting increasing attention from the scientific community. Numerous methods and techniques have been developed to address this issue, including adsorption [11], reverse osmosis [12], flotation [13], coagulation [14], ion exchange [15], chemical precipitation [16] and membrane filtration [17]. However, these techniques have several disadvantages, such as high operation costs, the use of a larger amount of chemicals, high sludge production, and secondary pollution [18,19]. Among the various remediation options, those based on material adsorption capabilities are recognized as the most promising for the removal of metals and micro-pollutants from natural and wastewater [20]. In fact, adsorption techniques are highly regarded due to their high efficiency, simplicity, low cost, and low environmental impact [21,22]. Hence, a variety of adsorbents like clay [23], activated carbon [24], zeolite [25], bentonite [26], graphene oxide [27], and cellulose [28] were applied to eliminate hazardous metal ions from aquatic systems. Among these adsorbents, mesoporous materials such as functional silica gel has gained considerable attention and owns its popularity to its high specific surface area, large pore size, low cost, feasibility, high thermal and mechanical stability, and low toxicity [29–32]. In addition, due to its high specific surface area (usually over 300 $m^2\ g^{-1}$) [33], tailored pore shapes and sizes, silica hybrid materials have already found application in the removal of hazardous metal ions [34], catalysis [35–37], and sensors [38]. In this context, the combination of mesoporous silicas with the porphyrin coordination chemistry can increase the adsorption capabilities of these materials and enhance specificity [39–45]. Indeed, the nitrogen atoms in the tetrapyrrolic core, due to their solid electron-donor properties, can act as ligand sites to attract metal ions and consequently allow their sensing or elimination with high efficiency [46,47]. Hence, the remarkable interest in porphyrin-functionalized silica hybrid materials is justified by their main characteristics, such as biocompatibility and high chemical resistance [48,49]. The multiple reuse and easy separation are the major benefits brought by these materials and can be combined with other treatments in a multi-barrier treatment line [50].

Density Functional Theory (DFT) calculations can explain relevant concepts and challenges found in different fields of chemistry [51–53], biology [54,55], and material sciences [56–58]. In line with this, DFT calculations have recently shown very good efficiency in understanding, interpreting, and predicting the behavior of a wide range of molecular properties involving metal coordination [59–67].

In this work, we describe the synthesis and the adsorption efficacy towards hazardous metal ions of two-novel inorganic-organic hybrid materials **Si3PyS** and **Si4PyS**, prepared by the functionalization of silica gel with porphyrin ligands substituted with three and four mercaptopyridyl units. The adsorption ability of the new hybrids with extra chelating units besides the porphyrin inner core was evaluated towards Cu^{2+}, Pb^{2+}, Cd^{2+} and Zn^{2+} ions in aqueous solutions. In this selection, we consider that these metal ions are common hazardous pollutants introduced into natural waters from different industries including those related to textiles, leather tanning, electroplating and metal finishing processes. Furthermore, the effects of pH, shaking time, kinetics, thermodynamic properties, selectivity, regeneration, and the application to real water were measured and discussed in detail. The electronic properties of **Si3PyS** and **Si4PyS** were investigated using DFT-B3LYP calculations, and the energies and the coordination sites of the materials with the hazardous metal ions were also evaluated.

2. Materials and methods

2.1. Synthesis of ligands L_1 and L_2

The porphyrins 5-(pentafluorophenyl)-10,15,20-tris(2,3,5,6-tetrafluoro-4-(pyridin-4-ylthio)phenyl)porphyrin (**L_1**) and 5,10,15,20-tetrakis(2,3,5,6-tetrafluoro-4-(pyridin-4-ylthio)-phenyl)porphyrin (**L_2**) were obtained from 5,10,15,20-tetrakis(pentafluorophenyl)porphyrin according with procedures reported in the literature [68–71].

2.2. Synthesis of 3-aminopropyl silica (SiPn)

Silica gel (Merck; 70–230 mesh, 60 Å) was activated before use by heating it at 120 °C for 24 h. Activated silica-gel (30 g) was dispersed in dried toluene (200 mL) in a two necked round bottom flask and refluxed with magnetic stirring under nitrogen atmosphere for 2 h. Subsequently, 3-aminopropyltrimethoxysilane (13 mL) was gradually added into the solution and refluxed for 24 h. The final product was filtered and washed sequentially with toluene and ethanol. The resulting solid was purified by Soxhlet extraction with a mixture of ethanol and dichloromethane (1:1) for 12 h, to remove the remain silylating agent [34,72]. Finally, the 3-aminopropylsilica (**SiPn**) was dried under vacuum at 40 °C for 24 h. The yield of 3-aminopropyl group grafted on the silica gel surface was 58%.

2.3. Synthesis of the inorganic-organic hybrids Si3PyS and Si4PyS

The preparation of **Si3PyS and Si4PyS**, involved the reflux in dry DMF (60 mL) of 3-aminopropylsilica prepared in the previous step (**SiPn**) (3 g) with porphyrin ligands **L_1** or **L_2** (ca. 200 mg) under nitrogen atmosphere during 48 h. Thereafter, the mixtures were allowed to cool to room temperature and the solids were filtered and transferred to a Soxhlet extraction apparatus for sequential reflux-extraction using DMF, ethanol and dichloromethane. UV–Vis analysis of the solutions resulting from the washing process did not show the presence of the free ligands **L_1** or **L_2** confirming their quantitative attachment to **SiPn**. The final materials **Si3PyS and Si4PyS** were dried under vacuum at 40 °C for 1 h.

2.4. Batch adsorption experiments

Batch experiments were performed in order to evaluate the impact of the contact time, pH and temperature in the adsorption process. Adsorption experiments were conducted under standard conditions, which were determined based on the effects of the adsorbent dose and concentration (data not shown). In the experiment, 10 mg of either **Si3PyS** or **Si4PyS** was stirred in 10 mL of an aqueous solution containing 200 mg L^{-1} of each metal salt [$Cu(NO_3)_2{\cdot}3H_2O$, $Pb(NO_3)_2{\cdot}6H_2O$, $Cd(NO_3)_2{\cdot}6H_2O$, and $Zn(NO_3)_2{\cdot}6H_2O$] in 50 mL flasks at room temperature. The pH values of the Cu^{2+}, Pb^{2+}, Zn^{2+}, and Cd^{2+} solutions were adjusted from 1 to 7 using diluted aqueous HCl or NaOH solutions. The effect of contact time was studied from 5 to 120 min at 25 °C and the optimum pH. The adsorption thermodynamics were investigated at different temperatures (25, 35, and 45 °C) for 30 min at optimum pH. After the removal of hazardous metal ions, the solid phase was separated by filtration using a 0.45 μm nylon membrane. The concentration of each metal ion was determined by atomic absorption measurements, and Eq. (1) was used to calculate the metal uptake in mg per unit mass of adsorbent:

$$q_e = (C_0 - C_e) \times \frac{V}{m} \quad (1)$$

where q_e (mg g^{-1}) is the adsorption amount, C_0 (mg L^{-1}) is the initial concentration, C_e (mg L^{-1}) is the final equilibrium concentration, V (L) is the volume of the solution, and m (g) represents the weight of the adsorbent.

These studies were not conducted with the ligands **L_1** or **L_2** before immobilization on **SiPn** because of their low solubility in water, which results in insoluble aggregates.

2.5. General remarks

^{13}C solid Nuclear Magnetic Resonance (NMR) spectra were recorded on a Bruker Avance III 400 spectrometer. Scanning electron microscopy (SEM - Hitachi S4100 equipped with energy dispersion spectroscopy) was used to characterize the silica particles. Brunauer–Emmett–Teller (BET)/Barrett–Joyner–Halenda (BJH) determination of the specific surface area and pore size distribution was achieved by using a Micromeritics Gemini 2380 surface area analyser with ca. 50 mg weight. Elemental analyses were performed on a LECO CHNS-932 apparatus. Attenuated Total Reflectance Transmission Fourier Transform Infrared (ATR-FTIR) spectra were registered on an FT Mattson 7000 galaxy series spectrophotometer. The nitrogen adsorption-desorption was obtained by means of a Thermoquest Sorpsomatic 1990 analyser. Solid UV–Vis absorption spectra in the spectral range 350–800 nm were registered using a JASCO V-560 spectrophotometer (JASCO International Co., Ltd., Tokyo, Japan). The mass loss determinations were performed in 90:10 oxygen/nitrogen atmosphere on a TGA Q50 V6.7 Build 203 instrument, at a heating rate of 10 °C min^{-1}. Atomic absorption measurements were performed at the University of Oujda, Morocco using a Spectra Varian A. A. 400 spectrophotometer. All the chemicals and solvents were of analytical grade and were used without further purification.

2.6. Computational details

The geometries of **Si3PyS** and **Si4PyS** were optimized using Gaussian 09 software [73] with the B3LYP approach [74] at the 6–31 G (d,p) basis set [75]. The surface analysis of the molecular electrostatic potential (MESP) have been carried out using MultiWFN [76] and VMD Software [77].

3. Results and discussion

3.1. Ligand synthesis

The ligands 5-(pentafluorophenyl)-10,15,20-tris(2,3,5,6-tetrafluoro-4-(pyridin-4-ylthio)phenyl)porphyrin (**L_1**) and 5,10,15,20-tetrakis (2,3,5,6-tetrafluoro-4-(pyridin-4-ylthio)-phenyl)porphyrin (**L_2**) were synthesized from 5,10,15,20-tetrakis(pentafluorophenyl)porphyrin according to a procedure previously reported in the literature [68–71]. The one pot synthesis was achieved via controlled nucleophilic aromatic substitution of three and four *p*-fluorine atoms from the starting scaffold (5,10,15,20-tetrakis(pentafluorophenyl)porphyrin) with 4 equivalents of 4-mercaptopyridine in the presence of diethylamine. Silica gel column chromatography with 5% MeOH/DCM was used to separate **L_1** from **L_2**.

The synthetic route to the new adsorbents is summarized in Scheme 1 and the first step involved the reaction of activated silica gel with 3-

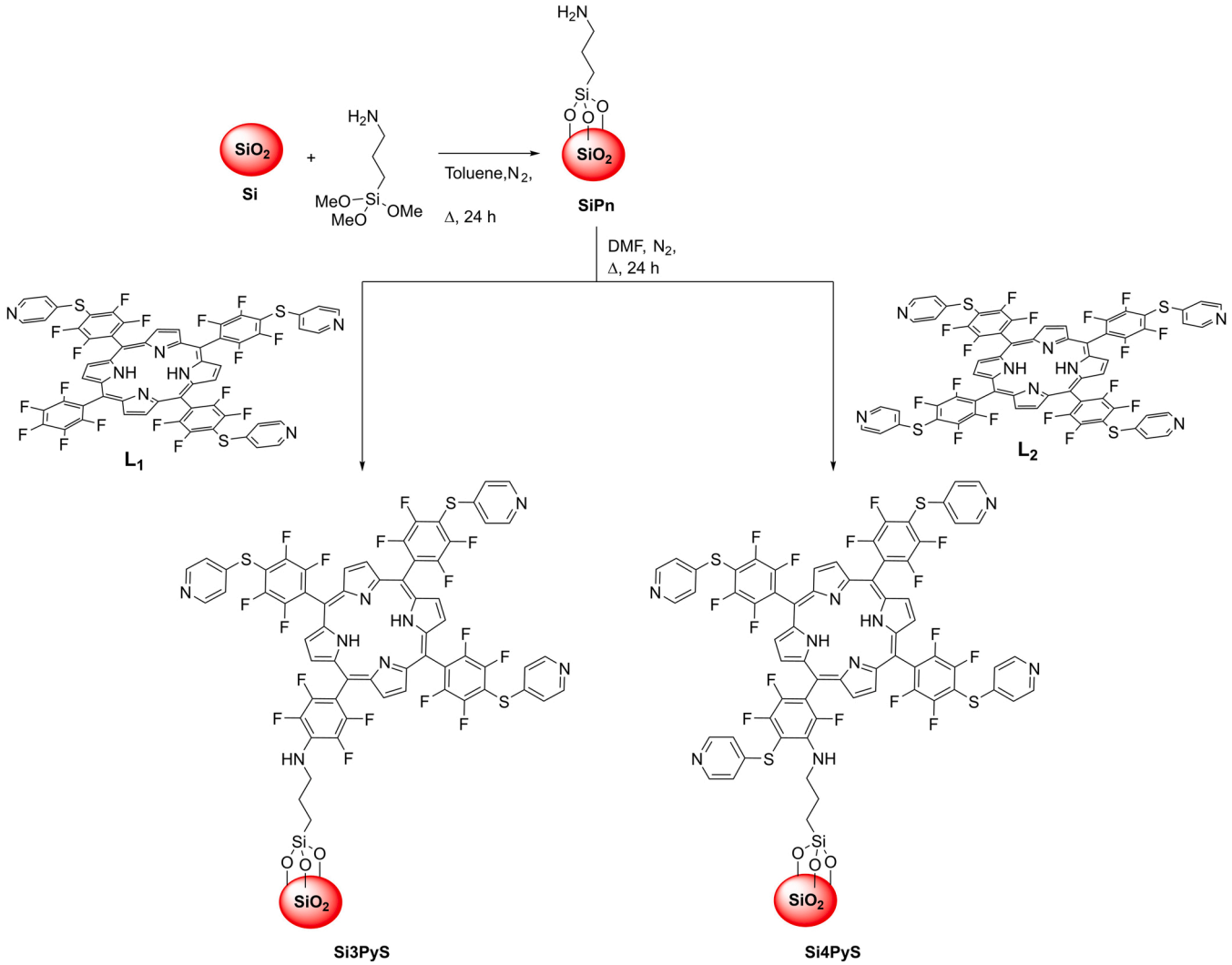

Scheme 1. Synthetic route to prepare the inorganic-organic hybrid materials **Si3PyS** and **Si4PyS**.

aminopropyltrimethoxysilane in dry toluene in order to introduce pendant amino groups on the silica surface [6]. The second step involved the reaction of the amino-functionalized silica with **L_1** or **L_2** in refluxing DMF for 48 h under a N_2 atmosphere. After this period, and a careful removal of any non-immobilized ligand by using a Soxhlet extraction in the presence of suitable solvents, the new chelating sorbent materials **Si3PyS** and **Si4PyS** were isolated as brown powders (Scheme 1). It is worth mentioning that porphyrin-based ligands **L_1** and **L_2** were successfully attached to the silica particles surface **SiPn** in almost quantitative yields. This was confirmed by the absence of porphyrin characteristic bands in the UV–Vis spectra of the organic solvents used to wash the new materials after the immobilization processes.

The attachments proposed were based on the reactivity in solution of 5,10,15,20-tetrakis(pentafluorophenyl)porphyrin with nucleophiles [78]. These reactions occur in a stepwise manner, with the *para* fluorine atoms being the first to be substituted. Therefore, we believe that for **Si3PyS**, the attachment to the silica surface via an amino bond occurred at the pentafluorophenyl ring non-substituted with pyridyl units. For **Si4PyS**, the attachment at the *meta* position was proposed considering that this position is less subjected to steric hindrance effects than the *ortho* positions because of the proximity of the porphyrinic core. Although, the possibility to occur di-substitution cannot be eliminated in both systems, we believe that the mono-substitution is the main process considering the diluted conditions used to do the ligand immobilization and the steric hindrance on porphyrins already linked to the silica surface.

3.2. Material characterization

3.2.1. Elemental analysis

The elemental analysis of carbon and nitrogen in **SiPn** allowed the identification of the relative percentages of the new elements introduced on the silica surface (Table 1). Thus, the **SiPn** microanalysis (%C = 5.03 and %N = 1.63) confirmed that the majority of the three methoxy groups were substituted by silanol. Considering the ^{13}C NMR analysis (vide infra Section 3.2.6) there are two distinct types of aminopropyl moieties fixation on the silica surface, bonds just with silanol groups and to a lesser extent involving a methoxy group (ratio of ca. 11:1). In addition, a further increase in the percentage of these elements was observed in the **Si3PyS** and **Si4PyS** materials. Accordingly, the C/N ratio is more significant than in **SiPn,** meaning that porphyrin ligands were successfully immobilized onto the silica surface throughout nucleophilic substitution reaction of fluorine atoms by the amino groups. In addition, Table 1 lists the grafting amount (A), in millimoles and milligrams of ligand per gram of silica, and the coverage of the silica surface was evaluated according to the Berendsen and Golan equation [79].

3.2.2. FTIR

The chemical modifications performed on the silica-gel materials were evaluated by FTIR spectroscopy (Fig. 1). The silica-gel alone (**Si**) exhibits the characteristic broad and intense bands attributed to the SiO–H stretching vibration at 3462 cm^{-1} and a band attributed to Si–OH, at 1638 cm^{-1} [6]. The intense bands at 1096 cm^{-1} and 972 cm^{-1} resulted from Si–O–Si stretching and Si-O vibrations [80]. By comparison the **SiPn** spectrum shows the expected peaks at 2979 cm^{-1} and 1563 cm^{-1}

Table 1
Elemental analysis of **SiPn**, **Si3PyS** and **Si4PyS**.

Sample	% C	% N	Ratio C/N	A (mmol of Ligand/g silica)	A (mg of Ligand/g silica)	Coverage degree (μmol m^{-2})
SiPn	5.03	1.63	3.09	-	-	-
Si3PyS	8.44	1.45	5.82	0.0482	60.16	3.52
Si4PyS	9.47	1.52	6.23	0.0578	76.31	4.47

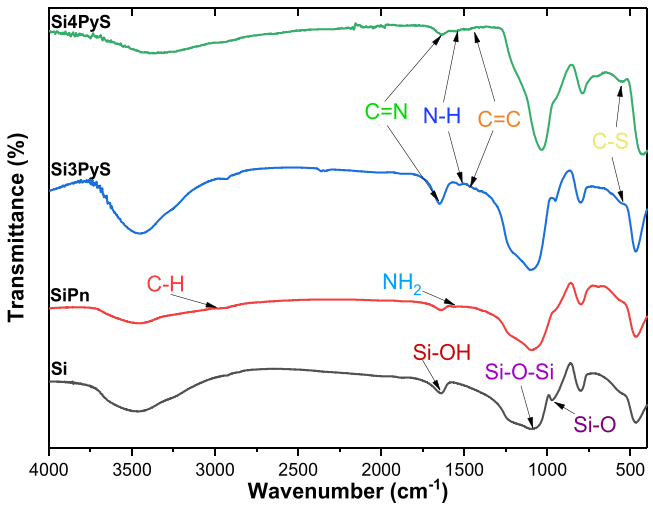

Fig. 1. FT-IR Spectra of silica-gel **(Si)**, 3-aminopropylsilica **(SiPn)**, and of the hybrids **Si3PyS** and **Si4PyS**.

corresponding to ν(C–H) and ν(NH_2) stretching vibrations ascribed to the newly introduced 3-aminopropylsilane moiety [81]. Consequently, the spectra of **Si3PyS** and **Si4PyS** materials reveal a band at 1541 cm^{-1} attributed to the vibration of the N-H bond of the secondary amine, and the appearance of new characteristic bands around 1647 cm^{-1}, 1469 cm^{-1} and 555 cm^{-1} results from the ν(C═N), ν(C═C) and ν(C-S) vibrations of the porphyrins **L_1** and **L_2**. These bands indicate the covalent successful grafting of these derivatives onto the silica-gel.

3.2.3. UV–Visible

The UV–Vis spectra of **L_1** and **L_2** both in liquid (recorded in DMSO at 298 K) and solid state are depicted in Fig. 2A and B. The comparison of the solid-state UV–vis spectra of both ligands **L_1** and **L_2**, and inorganic-organic hybrid materials **Si3PyS** and **Si4PyS,** exhibits the typical UV–Vis features of *meso*-tetraarylporphyrins with a strong Soret band at 416 (**L_1**) and 421 (**L_2**) nm followed by weaker absorption Q bands ranging from 509 to 678 nm (Fig. 2A). In comparison with the liquid state UV–Vis, the typical bands of **L_1** and **L_2** appear slightly red-shifted ca. 3 nm and the Soret band is much broader in the solid-state UV–Vis.

The analysis of the diffuse reflectance UV–Vis spectra of **Si3PyS** and **Si4PyS** confirms the successful grafting of **L_1** and **L_2** at the silica particle and the concomitant attainment of the intended inorganic-organic hybrids. The solid-state UV–Vis spectra of the hybrids **Si3PyS** and **Si4PyS** show a Soret band 5 nm blue-shift in the solid-state UV–Vis spectra of the corresponding free ligand, with absorption maxima at 414 and 419 nm, respectively. In contrast, a 6 nm red-shift in the Q-bands region was observed after the immobilization of **L_1** and **L_2**.

3.2.4. XRD analysis

Fig. 3 shows the XRD patterns of free silica **Si**, 3-aminoproyl-silica **SiPn**, **Si3PyS** and **Si4PyS**. In both hybrids, the peak of diffraction (110) shows a step decrease of intensity when compared with **Si** or **SiPn** indicating that the incorporation of organic groups affected the structure of the pores. Additionally, a relatively broad diffraction peak at low 2θ was observed after grafting the organic moieties on silica gel surface. Furthermore, the reduction in peak intensity can be ascribed to the decline in silica content following immobilization. The increase in porphyrin concentration (mmol g^{-1}), which can cause a decrease in the silica content within the structure, may lead to a reduction in intensity. This is agreement with the successful modification of silica gel by the organic ligands.

3.2.5. Scanning electron micrographs

Fig. 4a-d compares the scanning electron microscopy (SEM) images

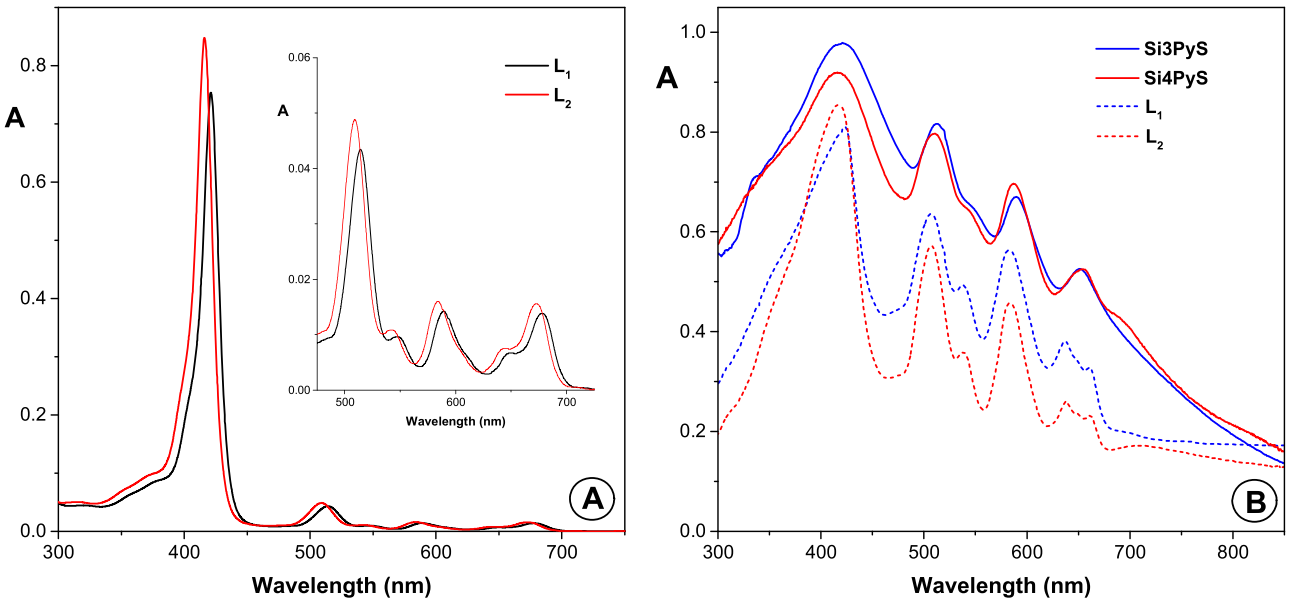

Fig. 2. (A) Absorption spectra of $\mathbf{L_1}$ and $\mathbf{L_2}$ in DMSO at 298 K ($[\mathbf{L_1}] = [\mathbf{L_2}] = 3 \times 10^{-6}$ M) and (**B**) solid-state UV–vis spectra of **Si3PyS** and **Si4PyS** (solid lines) and of ligands $\mathbf{L_1}$ and $\mathbf{L_2}$ (short dashed lines).

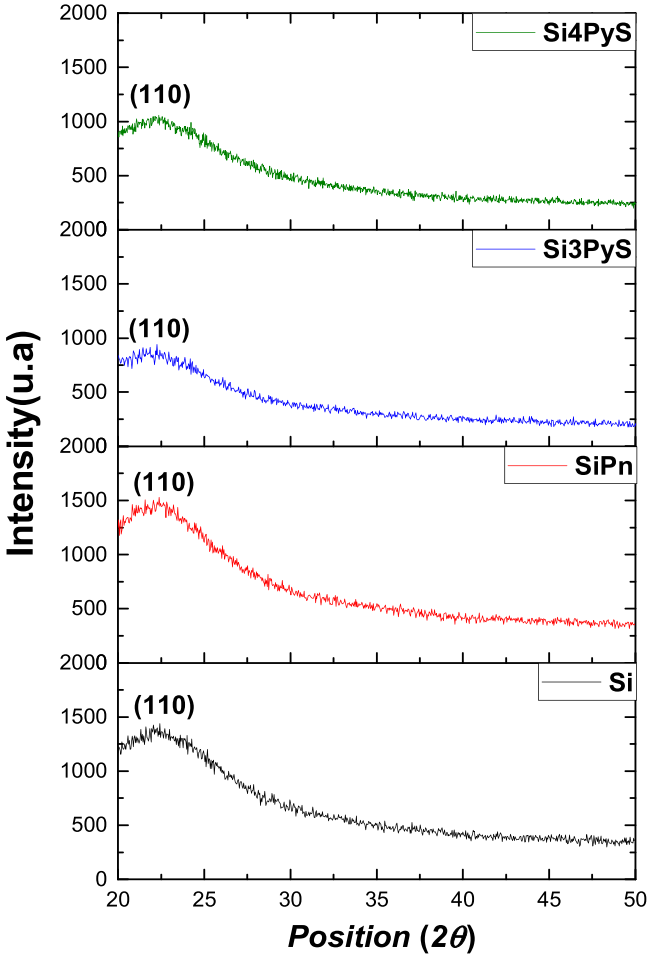

Fig. 3. X-ray diffraction patterns of free silica **Si**, aminopropyl-silica **SiPn** and the materials **Si3PyS** and **Si4PyS**.

recorded for the non-functionalized silica **Si**, the amino-functionalized silica **SiPn** and silica-based hybrids **Si3PyS** and **Si4PyS**. From the morphological analysis, it was possible to observe a significant decrease in the silica-based particle size after their functionalization with $\mathbf{L_1}$ and $\mathbf{L_2}$. The higher amount of organic components leads to partial aggregation of inorganic-organic hybrid particles.

Also, a significant increase of the surface roughness is noticeable in the functionalized **Si3PyS** and **Si4PyS** hybrid materials when compared with **Si** and **SiPn** whose surfaces are much smoother. This morphology was confirmed by the analysis of magnified **Si3PyS** and **Si4PyS** particles using SEM and scanning transmission electron microscopy (STEM), which are very sensitive to variations in the surface structure (Fig. 4e-h).

It is worth emphasizing that rough surfaces generally exhibited better metal cation adsorption features [82]. The roughness displayed by the inorganic-organic hybrid materials **Si3PyS** and **Si4PyS** is also an indication of a successful grafting of the porphyrin-based ligands $\mathbf{L_1}$ and $\mathbf{L_2}$ onto the silica surface.

3.2.6. *^{13}C NMR solid state*

The novel hybrid materials **Si3PyS** and **Si4PyS** were also characterized by solid state ^{13}C NMR spectroscopy and the resulting spectra are shown in Fig. 5; for comparison the spectrum of **SiPn** is also depicted in the same figure. The signals observed for 3-aminopropylsilica **SiPn** at δ 9.8, δ 23.1 and δ 42.8 ppm were assigned to the resonances of the propyl carbon Si-CH_2, -CH_2- and *N*-CH_2, respectively. The peak at δ 48.05 ppm may be attributed to the carbon resonance of some methanol (resulting from the hydrolysis of 3-aminopropyltrimethoxysilane) adsorbed on the **SiPn**. The signal at δ 51.1 ppm was assigned to the resonance of the non-substituted methoxy carbon (–OCH_3) in which the pendant aminopropyl arm is linked by only two silanol bonds (represent less than 10%) [83]. For the materials **Si3PyS** and **Si4PyS**, the signals of silica backbone are accompanied with new signals appearing between δ 109.1 and δ 164.1 ppm corresponding to the resonance of the aromatic carbons of the porphyrinic entities.

3.2.7. *TGA analysis and thermal stability*

The thermal stabilities of the final materials **Si3PyS** and **Si4PyS** were determined by thermogravimetric analysis and the results were compared with those obtained for **Si** and **SiPn** (Fig. 6). The first loss of 2.75% observed for free silica (**Si**) in the range between 25 and 110 °C is

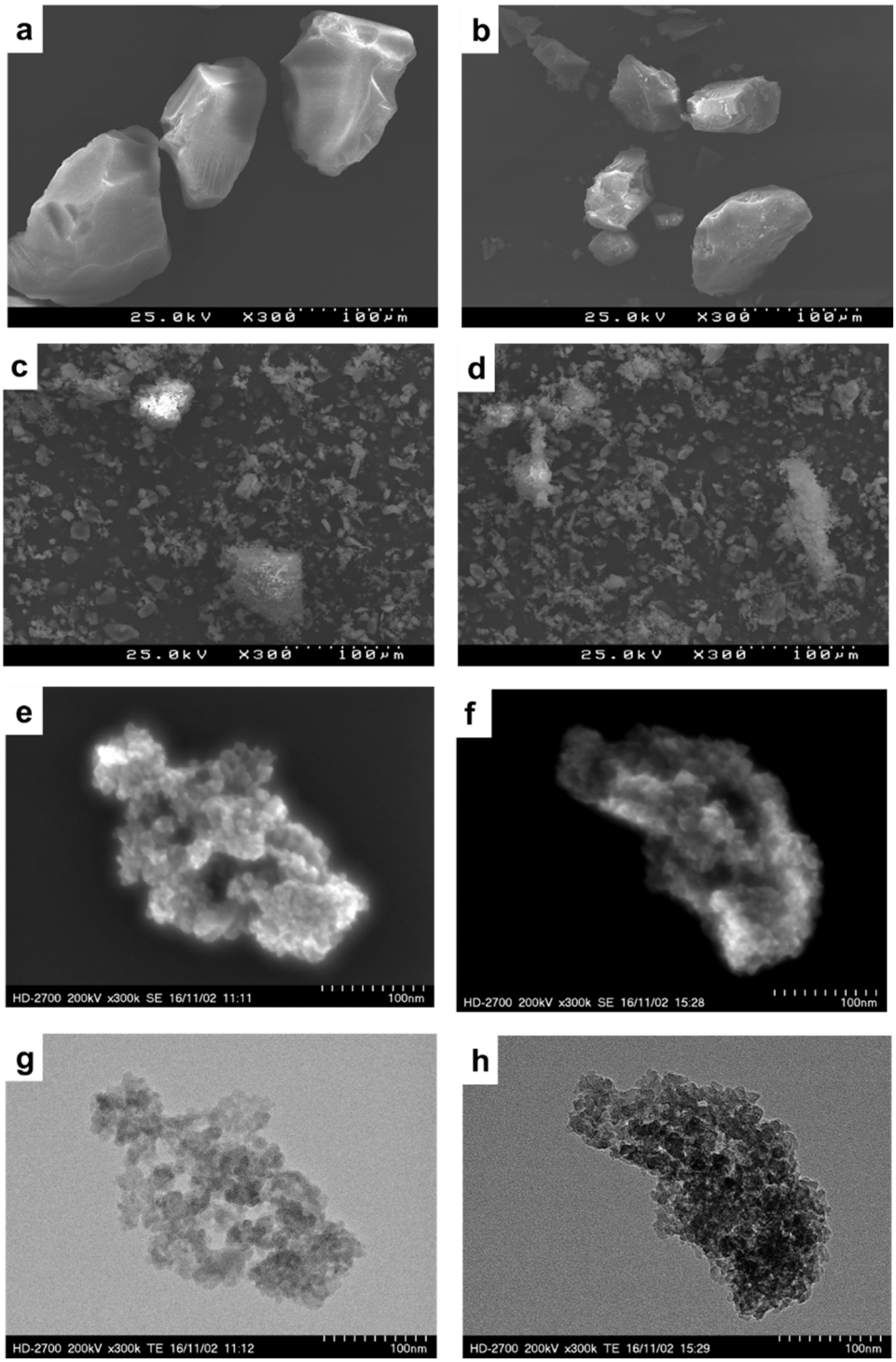

Fig. 4. SEM images of free silica **Si** (a), **SiPn** (b), **Si3PyS** (c), and **Si4PyS** (d) at x300 magnification. SEM (e and f) and STEM images of **Si3PyS** (g) and **Si4PyS** (h) at an x300K magnification.

attributed to the release of physiosorbed water molecules and the second loss of 0.89% from 110 to 800 ºC to the condensation of silanol groups bonded to the surface [84,85]. The 3-aminopropyl-silica (**SiPn**) presents an additional weight loss, after the drainage of physically adsorbed water, mainly due to the presence of the extra organic arm. The final materials **Si3PyS** and **Si4PyS**, also showed an increase of mass loss due to the decomposition of the porphyrin immobilized on the surface of silica gel, with condensation of the remaining silanol groups. This increase in mass loss reflects the high amount of the anchored organic groups.

3.2.8. *Surface properties*

Fig. 7 shows the nitrogen adsorption–desorption isotherms for **SiPn**, **Si3PyS** and **Si4PyS**, which are of type IV and clearly indicate mesoporous features. The volume adsorbed on silica increased steeply at a relative pressure of $P/P_0 \sim 0.7$, which represents capillary condensation of nitrogen within the uniform mesoporous structure. The inflection position is shifted towards lower relative pressures and nitrogen volume

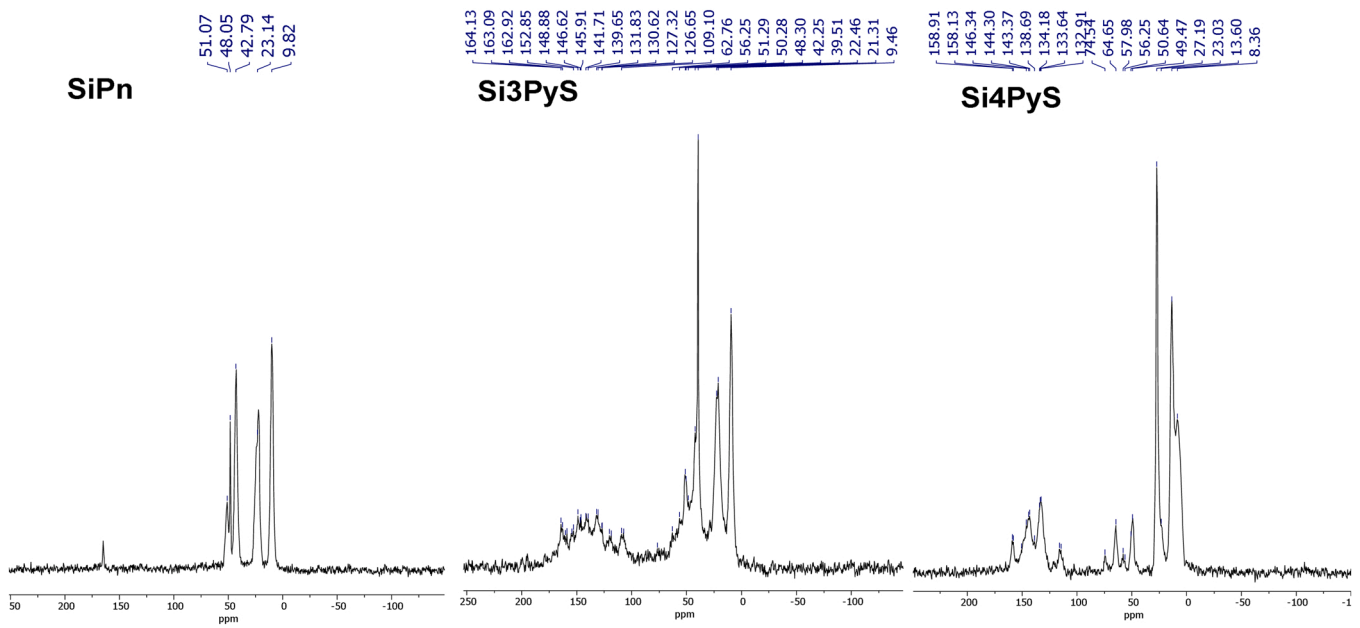

Fig. 5. Solid ^{13}C NMR spectra of **SiPn**, **Si3PyS** and **Si4PyS.**

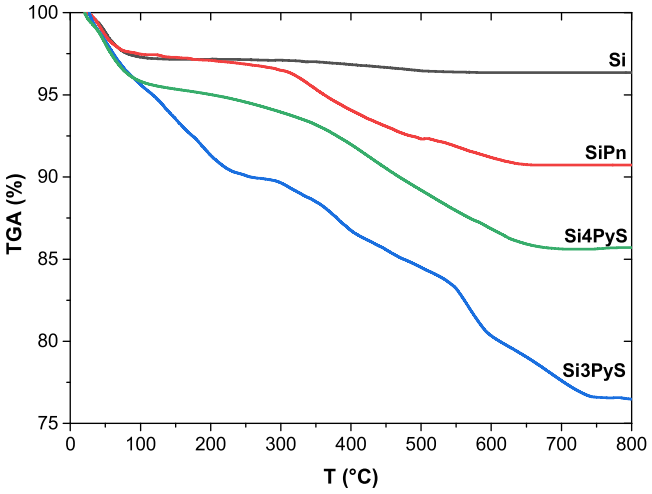

Fig. 6. Thermogravimetric curves of free silica **Si**, **SiPn**, **Si3PyS** and **Si4PyS**.

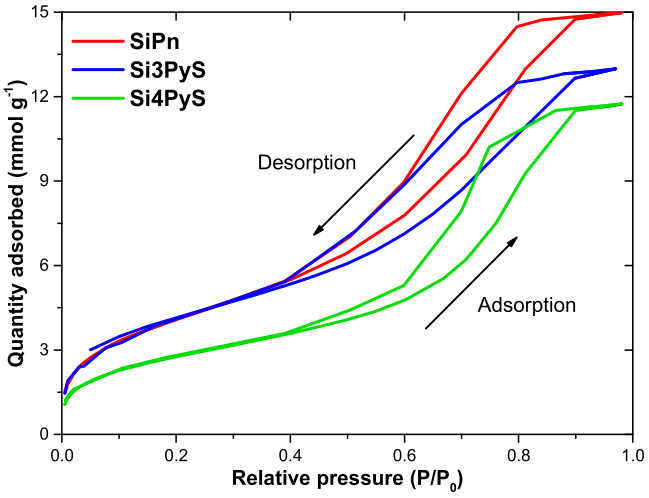

Fig. 7. Nitrogen adsorption–desorption isotherm plots of **SiPn**, **Si3PyS** and **Si4PyS**.

decreases with functionalization [86]. The density of the pendant groups covalently attached to the inorganic silica backbone changes the original characteristics of the surface. Thus, the initial specific surface area (S_{BET}) of 434.65 ± 4.61 m^2 g^{-1} (**Si**) decreases as the immobilization takes place to give 328.75 ± 5.56 m^2 g^{-1} (**SiPn**). A decrease in S_{BET} is mainly due to the presence of the organic moieties that can block the access nitrogen to the silica base. On the other hand, we observed that **Si3PyS** and **Si4PyS**, has a supplementary decrease BET surface area as additional groups immobilization takes place to give 259.82 ± 12.97 m^2 g^{-1} and 222.97 ± 1.89 m^2 g^{-1}, respectively. In addition, the average pore size 46.358 Å (**SiPn**), 57.488 Å (**Si3PyS**) and 63.199 Å (**Si4PyS**) increased after the modification as a result of clogging in the smaller pores. It can be inferred that the surface roughness has increased, as evidenced by SEM imaging, or to the pore plugging of the support by the ligand. The changed surface area in **Si3PyS** and **Si4PyS**, are therefore attributable to the grafted of porphyrin ligands where the presence of the extra mercaptopyridyl unit in **Si4PyS** in the fluorophenyl linkage unit is probably responsible by a slightly less effective blockage of the mesopores of the silica-gel. This difference in the unit linkage is corroborated by the thermogravimetric analysis where an extra weight loss (ca 10%) at higher temperatures is observed for **Si3PyS** when compared with **Si4PyS** (Fig. 6).

3.3. *Adsorption studies*

3.3.1. *pH effect*

The influence of pH on the adsorption of Cu^{2+}, Pb^{2+}, Zn^{2+} and Cd^{2+} by **Si3PyS** and **Si4PyS** was investigated in the range from 1 to 7 and the results presented in Fig. 8 show that removal of the metals increases with the increase in solution pH. The maximum removal of Cu^{2+}, Pb^{2+}, Zn^{2+} and Cd^{2+} was observed at a pH values between 6 and 7. At lower pH values, the retention of hazardous metal ions by the functionalized silica (**Si3PyS** and **Si4PyS**) is not significant since the porphyrinic receptor must be almost entirely in its protonated form and a low interaction or strong electronic repulsion forces occur between the donor atoms and the metal ions. At neutral pH, the contribution of the cationic forms is less significant, favouring the interactions between the non-protonated

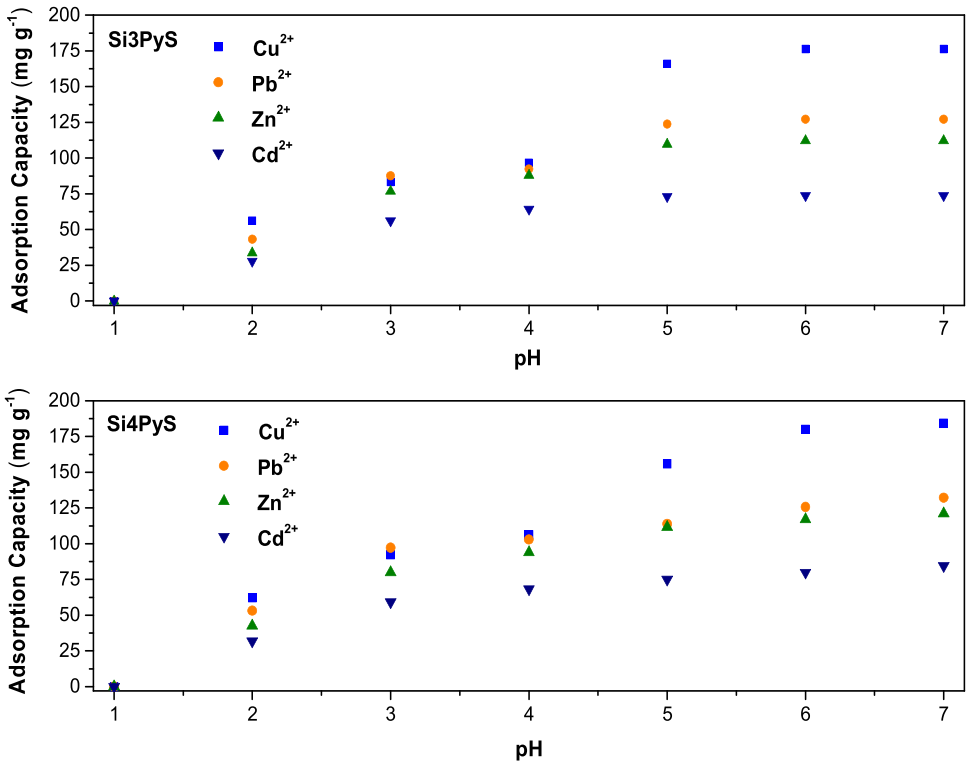

Fig. 8. Effect of pH on the adsorption of metal ions on **Si3PyS** and **Si4PyS**. (Experimental conditions: $C_0 = 200$ mg L^{-1} in each case, $t_{contact} = 30$ min and T = 25 °C).

donor atoms and the metal ions, which enhances the chelation and adsorption of metal ions. At a pH higher than 7, the retention of metal ions decreased due to the hydrolysis of metal ions affording the corresponding hydroxides ($M(OH)_2$). Indeed, pH = 6 is the optimum pH for the maximum sorption of Cu^{2+}, Pb $^{2+}$, Zn^{2+} and Cd^{2+} (vide infra Table 2).

3.3.2. *Effect of contact time and adsorption kinetics*

A rapid adsorption time helps to reduce capital and costs, particularly in natural waters where the metal ions content is low. Therefore, the contact time was investigated in a range from 5 to 30 min at room temperature (25 °C), using the best conditions previously established (10 mg of adsorbent, metal concentrations of $C_0 = 200$ mg L^{-1} and pH = 6). The effect of the contact time on the extraction of Cu^{2+}, Pb^{2+}, Zn^{2+}, and Cd^{2+} by **Si3PyS** and **Si4PyS** is shown in Fig. 9. In both cases a rapid increase of their adsorption capacity is noticed in the first 5 min of contact and, in general, the equilibrium is reached at 10–15 min. Such fast kinetics will benefit highly efficient metal adsorption.

To better understand adsorption kinetics of **Si3PyS** and **Si4PyS**, mathematical kinetic models such as the pseudo-first-order and pseudo-second order kinetic models [87–90] were applied to the experimental data. The nonlinear form of the pseudo-first order kinetic mathematical expression and of the nonlinear form pseudo-second-order model are expressed by Eqs. (2) and (3):

$$q_t = q_e\left[1 - e^{-K_1 t}\right] \tag{2}$$

$$q_t = \frac{k_2 q_e^2 t}{1 + k_2 q_e t} \tag{3}$$

where q_e (mg g^{-1}) and q_t (mg g^{-1}) are the equilibrium adsorption amount and the adsorption capacity over a period of time, and k_1 (min^{-1}) is the rate constant of the first order adsorption while k_2 (g mg^{-1} min^{-1}) is the pseudo-second-order adsorption rate constant.

The results are presented in Fig. 9 and the fitting parameters of the two models are listed in Table 2. A fine analysis suggests that the pseudo-second-order model is more suitable for describing the kinetic adsorption process of Cu^{2+}, Pb^{2+}, Zn^{2+} and Cd^{2+}. This phenomenon can be explained by the availability of active sites on the surface of **Si3PyS** and **Si4PyS** adsorbents, which become occupied at 25 min by metal cations. Furthermore, the results obtained from this model indicate that a chemisorption mechanism, involving complexation reaction shared between the adsorbate and adsorbent is the more effective adsorption pathway.

Table 2
Kinetics of metal ions removal by **Si3PyS** and **Si4PyS**.

Materials	Metal ions	q_e, exp (mg g^{-1})	Pseudo-first-order			Pseudo-second-order		
			q_e, cal (mg g^{-1})	k_1 (min^{-1})	R^2	q_e, cal (mg g^{-1})	k_2 (g mg^{-1} min^{-1})	R^2
Si3PyS	Cu^{+2}	176.32	171.789 ± 1.867	0.537 ± 0.077	0.996	177.477 ± 1.901	0.009 ± 0.002	0.998
	Pb^{+2}	127.18	123.492 ± 1.716	0.435 ± 0.057	0.993	129.787 ± 1.496	0.008 ± 0.001	0.998
	Zn^{+2}	112.08	110.895 ± 0.591	0.457 ± 0.024	0.999	115.253 ± 0.276	0.011 ± 0.001	0.999
	Cd^{+2}	73.84	72.722 ± 0.566	0.415 ± 0.029	0.998	76.332 ± 0.224	0.011 ± 0.001	0.999
Si4PyS	Cu^{+2}	184.16	181.819 ± 1.195	0.570 ± 0.055	0.998	186.501 ± 0.779	0.011 ± 0.001	0.999
	Pb^{+2}	132.16	130.527 ± 0.888	0.488 ± 0.037	0.998	135.164 ± 0.322	0.011 ± 0.001	0.999
	Zn^{+2}	112.07	111.64 ± 0.475	0.871 ± 0.164	0.999	111.961 ± 0.816	0.146 ± 0.179	0.999
	Cd^{+2}	84.54	82.415 ± 0.854	0.534 ± 0.072	0.996	85.158 ± 0.798	0.020 ± 0.003	0.998

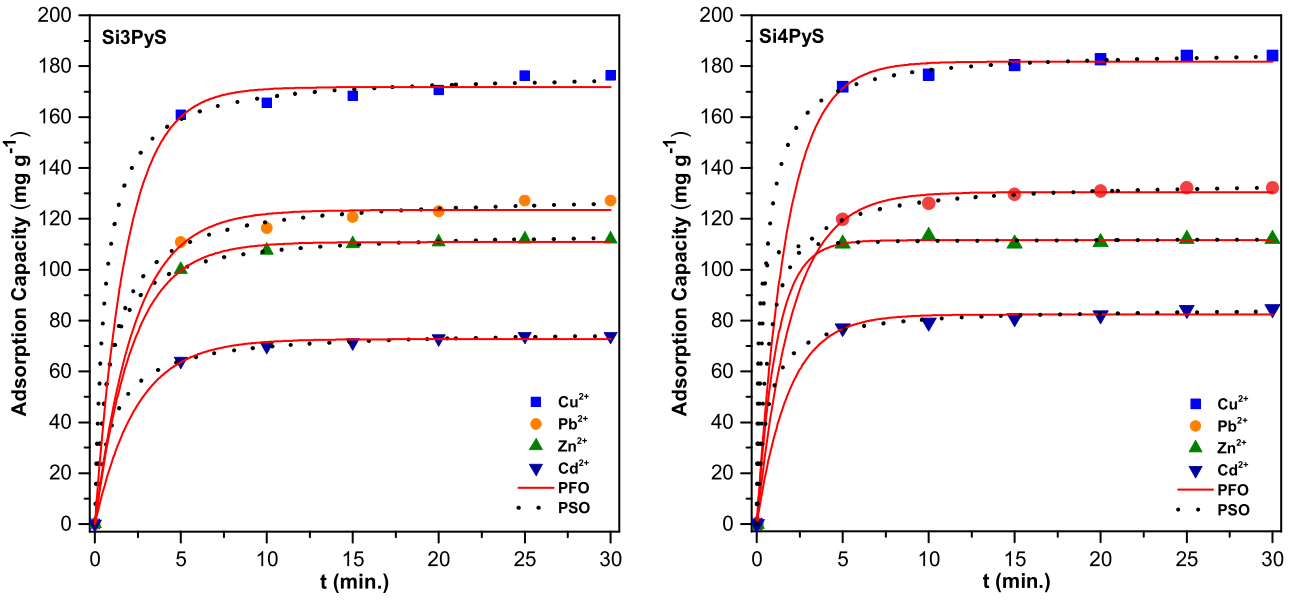

Fig. 9. Pseudo-first-order (PFO) and pseudo-second-order (PSO) models fit for the adsorption of Cu^{2+}, Pb^{2+}, Zn^{2+} and Cd^{2+} by **Si3PyS** (left) and **Si4PyS** (right) (experimental conditions: V = 10 mL, m = 10 mg of adsorbent, C_0 = 200 mg L^{-1} in each case and T = 25 °C).

3.3.3. *Thermodynamic modeling*

Thermodynamic parameters are crucial for determining the spontaneity of an adsorption process. The thermodynamic of metal ions sorption onto **Si3PyS** and **Si4PyS** from aqueous solution were studied between 25 and 45 °C, the Standard Gibbs free energy changes (ΔG^0), enthalpy change (ΔH^0), and entropy change (ΔS^0) were determined using the following equations [91]:

$$K_d = \frac{C_0 - C_e}{C_e} \times \frac{V}{m} \quad (4)$$

$$\Delta G = \Delta H - T\Delta S \quad (5)$$

$$\ln K_d = \frac{-\Delta H}{RT} + \frac{\Delta S}{R} \quad (6)$$

where R (8.314 J mol^{-1} K^{-1}) is the gas constant, M (g mol^{-1}) is the molar mass, T (K) is the temperature, K_d is the distribution coefficient, C_0 (mg L^{-1}) is the initial concentration of metal ion, and C_e (mg L^{-1}) is the equilibrium concentration of metal ion, V is the volume of solution and m (g) is the dosage of sorbents.

The results are shown in Fig. 10 and the values of various thermodynamic parameters obtained for the adsorption process of each hybrid for different hazardous metal cations are summarized in Table 3. The positive values of ΔH^0 indicate an endothermic adsorption process leading to a temperature increase that promote metal cation (Cu^{2+}, Pb^{2+}, Zn^{2+} and Cd^{2+}) adsorption by **Si3PyS** and **Si4PyS**. In addition, positive ΔS^0 values reveal an increased randomness at the solid–solution

Table 3
Values of various thermodynamic parameters for adsorption of heavy metals on **Si3PyS** and **Si4PyS**.

Materials	Metal ions	ΔH° (kJ mol^{-1})	ΔS° (J K^{-1} mol^{-1})	ΔG° (kJ mol^{-1})		
				299.15	309.15	319.15
Si3PyS	Cu^{2+}	11.31	45.71	-2.366	-2.823	-3.280
	Pb^{2+}	13.50	47.93	-0.839	-1.318	-1.797
	Zn^{2+}	11.16	38.97	-0.493	-0.884	-1.274
	Cd^{2+}	13.12	54.41	-3.151	-3.695	-4.239
Si4PyS	Cu^{2+}	8.374	38.768	-3.22	-3.60	-3.99
	Pb^{2+}	7.097	31.316	-2.26	-2.58	-2.89
	Zn^{2+}	6.662	28.875	-1.97	-2.26	-2.55
	Cd^{2+}	6.878	35.860	-3.84	-4.20	-4.56

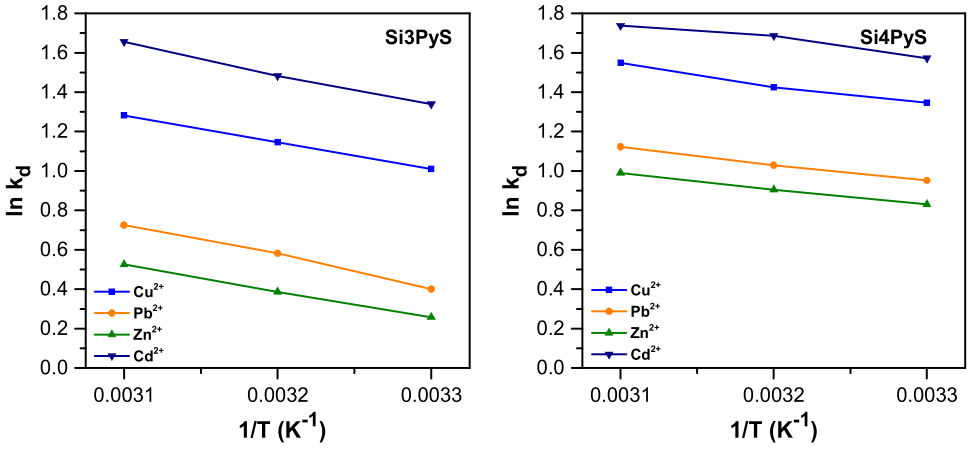

Fig. 10. Temperature effect on the sorption of metal ions by **Si3PyS** and **Si4PyS** (Experimental conditions: t = 30 min, pH = 6, C_0 = 200 mg L^{-1} in each case and adsorption dose: V =10 mL, m = 10 mg of **Si3PyS** and **Si4PyS**).

interface during the adsorption processes while negative values of ΔG^0 indicate a spontaneous process where the adsorption is thermodynamically favorable. Furthermore, the ΔG^0 values of the **Si4PyS** material are lower than those of **Si3PyS**, which may be due to the presence of an additional mercaptopyridine that facilitates the coordination of Cu^{2+} ions.

3.3.4. Selectivity

The assays to evaluate the selectivity of **Si3PyS** or **Si4PyS** towards the different metals were performed in aqueous solutions containing the mixed Cu^{2+}, Pb^{2+}, Zn^{2+}, Cd^{2+} quaternary system at the optimal concentration for each metal ions; all these experiments were performed under batch conditions at room temperature and at the optimal pH. The results illustrated in Fig. 11, show that both materials (**Si3PyS** and **Si4PyS)** exhibit an excellent Cu^{2+} adsorption and affinity. However, the extraction efficiency seemed to decrease when compared to the values obtained in the absence of foreign metal ions (see Table 2). The high affinity towards Cu^{2+} may be linked to the small hydrated ionic radius of Cu^{2+} when compared to other hazardous metal ions with higher hydrated ionic radii since the active sites are more difficult to reach. However, the remarkable selectivity toward Cu^{2+} favors these materials as promising adsorbent, for the removal of Cu^{2+} from aqueous solutions containing competing ions.

3.3.5. Extraction of hazardous metal in natural real water and industrial wastewater samples

This study was performed to evaluate the capability of **Si3PyS** and **Si4PyS** on the removal of Cu^{2+}, Pb^{2+}, Zn^{2+} and Cd^{2+} in real conditions. The water samples used in this study were collected from the Moulouya River (Morocco) to represent natural water, and from the Industrial Zone of Oujda (Morocco) to represent industrial wastewater. All samples were collected under standard conditions (polyethylene bottle, filtered through a 0.45 μm nylon membrane and used without storage). The applicability of **Si3PyS** and **Si4PyS** in copper removal was determined using the batch method by mixing 10 mg of the adsorbent with 10 mL of the samples at room temperature. To the natural real water samples, free of Cu^{2+} ions, we have added this metal ion at a concentration of 10 mg L^{-1}. Analyses were performed in duplicate for each sample. The results illustrated in Table 4 shows that the organic matter and alkali metals, which naturally exist in natural water or industrial wastewater, do not interfere with the materials extraction capabilities towards Cu^{2+}.

Table 4
Experimental data obtained from adsorption assays to remove hazardous metal ions from natural real water samples and industrial wastewaters.

Samples	Metal ions	$C_{found} \pm 0.05$ (mg L^{-1})	Adsorption capacity (mg g^{-1})	
			Si3PyS	Si4PyS
Moulouya River	Cu^{2+}	7.51	5.70	6.00
	Cd^{2+}	0.313	0.274	0.290
	Pb^{2+}	0.979	0.320	0.380
	Zn^{2+}	N.D.	-	-
Industrial wastewater	Cu^{2+}	47.52	47.09	47.14
	Cd^{2+}	0.52	0.44	0.49
	Pb^{2+}	1.11	0.67	0.89
	Zn^{2+}	39.47	39.41	39.31

C_{found} is the initial metal contents in river water determined by atomic absorption measurements. N.D. – not detectable.

3.3.6. Renewability

Both adsorbents **Si3PyS** and **Si4PyS** were easily regenerated by washing them with an acidic solution for a few minutes (5 −10 mL of 6 N HCl per g of support). The regenerated solids presented good stability and could be reused several times without decreasing its extraction efficiency. The stability of the organic groups onto the solid surface was also confirmed by TGA (Fig. 12), with no distinct changes in the sorbent material after five cycles of utilization. Moreover, the materials are found to be stable after five cycles of adsorption-desorption, with no significant change in the percentages of adsorption, which remained around 98% in each cycle (Table 5). This information highlights the potential of these materials to be used repeatedly for the removal of Cu^{2+} ions without significant loss of their adsorption capacity or stability.

3.3.7. Adsorption mechanism

The sorption efficiency of **Si3PyS** and **Si4PyS** towards the different metal ions can be explained by their coordination with the nitrogen atoms present either at the inner core of the macrocycle but also at the pendant mercaptopyridyl units. The results showed that the presence of the extra ligands was particularly relevant for improving the sorption performance of the starting scaffold 5,10,15,20-tetrakis(pentafluorophenyl)porphyrin towards Cu^{2+}. In the literature, this metal ion prefers to be coordinated by four donor atoms [92]. Therefore, peripheral donor nitrogen moieties, as well as nitrogens at the porphyrin inner core are the responsible on the coordination of Cu^{2+} [93]. Interesting, this

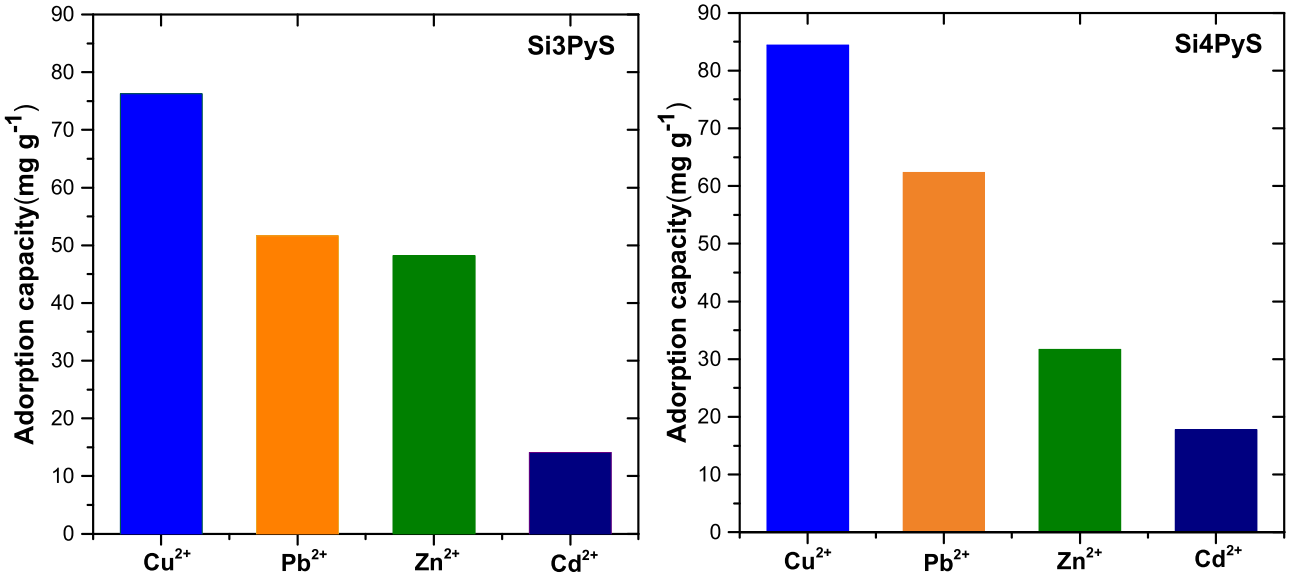

Fig. 11. Foreign metal ions effect on Cu^{2+} removal using **Si3PyS** and **Si4PyS**.

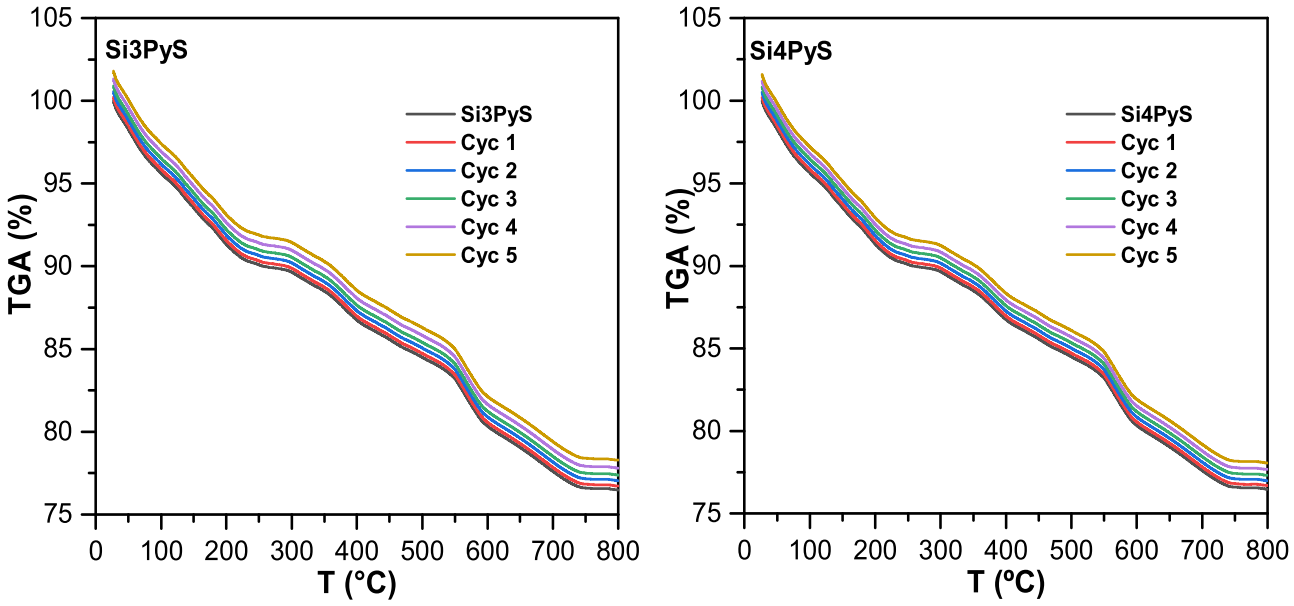

Fig. 12. Thermogravimetric curves of adsorbents **Si3PyS** and **Si4PyS** before and after five cycles of regeneration.

Table 5
Adsorption-desorption cycles of hybrid materials towards Cu^{2+}.

Cycles	Cu^{2+} adsorption capacity (mg g^{-1})		% of efficiency between cycles	
	Si3PyS	Si4PyS	Si3PyS	Si4PyS
1	175.98	184.05	100	100
2	175.16	184.00	99.5	100
3	173.80	183.23	98.8	99.6
4	173.62	182.83	98.6	99.3
5	173.32	182.56	98.5	99.1

sorption capacity by the inorganic-organic sorbent **Si4PyS** is higher when compared to the one displayed by the analog **Si3PyS** (184.16 mg g^{-1} vs 176.32 mg g^{-1}, respectively). This may be attributed to the reinforcement of the Cu^{2+} complexation ability of the porphyrin macrocycle when is decorated with four mercaptopyridine units instead of three of these units (Fig. 13).

3.3.8. *Comparison with alternative adsorbents*

Table 6 shows the adsorption of Cu^{2+} by other adsorbents reported in the literature. Both porphyrin-silica adsorbents described in this work show an improved adsorption capability. The remarkable affinity for Cu^{2+} adsorption of inorganic-organic hybrids **Si3PyS** and **Si4PyS** compared to the other adsorbents described in the literature is highlighted by their ability to adsorb approximately more 29–32% than the silica-supported sorbent based on the starting scaffold 5,10,15,20-tetrakis(pentafluorophenyl)porphyrin reported by our group and 99.6% more than 4-amino-2-mercaptopyrimidine.

The absorption capability of both inorganic-organic hybrids, along with the improvements attained in recent years concerning the synthesis of *meso*-tetraarylporphyrins with more efficient preparation methods and higher yields, emphasizes the potential of this family of materials. To make the application economically viable on a higher scale, it is required to gather the knowledge of multidisciplinary teams capable of optimizing the synthesis and modification of this type of derivatives with adequate binding motifs aiming to increase their removal features. In fact, this study shows that the use of cheap supports, such as silica gel functionalized with porphyrin-based ligands, has a high potential to be

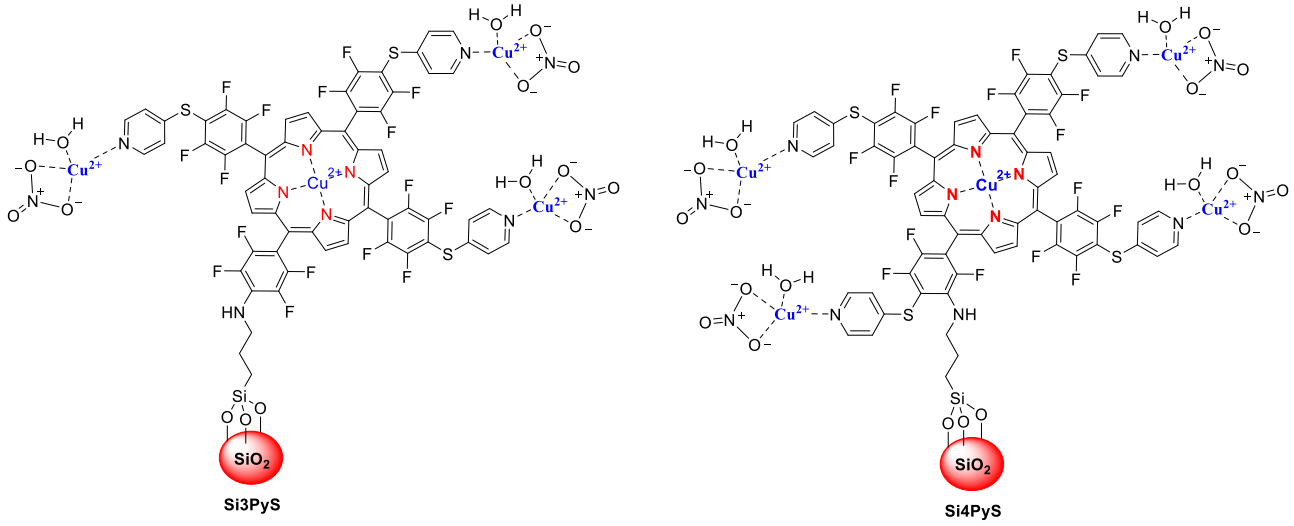

Fig. 13. Schematic representation of the proposed binding mode to attain Cu(II) complexes formed on the surface of **Si3PyS** and **Si4PyS**.

Table 6
Comparison of **Si3PyS** and **Si4PyS** performances with some recently reported sorbents for Cu^{2+} adsorption.

Sorbents	Ref.	Adsorption capacity (mg g^{-1})
5-(Pentafluorophenyl)-10,15,20-tris(2,3,5,6-tetrafluoro-4-(pyridin-4-ylthio)phenyl)porphyrin (**Si3PyS**)	**This work**	**176.32**
5,10,15,20-Tetrakis(2,3,5,6-tetrafluoro-4-(pyridin-4-ylthio)phenyl)porphyrin (**Si4PyS**)	**This work**	**184.16**
5,10,15,20-Tetrakis(pentafluorophenyl)porphyrin	[83]	125.17
β-Ketoenol-bipyridine	[94]	131.82
Pyridylpyrazole-β-ketoenol	[95]	63.05
β-Keto-enol bis-heterocycle	[96]	27.35
Pyridine-2,6-dicarbaldehyde	[97]	120.65
1-(Furan-2-yl)imine	[98]	77.48
Bis(pyrazole)butane	[99]	20.24
(2*Z*)-1-(1,5-Dimethyl-1*H*-pyrazol-3-yl)-3-hydroxybut-2-en-1-one	[100]	71.43
β-Keto-enol-bisfuran	[101]	44.10
β-Ketoenol-pyridine-furan	[102]	32.15
Schiff base tailed silatranes	[80]	13.15
Stearic acid	[103]	63.87
N-[3-(trimethoxysilyl)propyl]ethylene-diamine (TPED)	[104]	27.22
Brazilian Orchid Tree	[105]	8.89
Corn Leaf Powder	[106]	5.65
4-Amino-2-mercaptopyrimidine	[107]	0.76
p-Morpholinomethylcalix[4]arene bonded silica	[108]	1.652
Polyhexamethylene guanidine-Arsenazo I	[109]	3.812
2,3-Dihydroxybenzaldehyde	[110]	6.04
3-(2-Aminoethylamino)propyldimethoxymethylsilane	[111]	74.69
N,N-bis(thiophen-1-ylmethyl)amine	[112]	51.14
5-Nitrothiophene-2-carbaldehyde	[113]	67.56

explored as adsorbents. The quantitative attachment of porphyrinic ligands on the silica surface allowed the formation of new organic-inorganic hybrids with excellent removal capabilities, when compared with other adsorbents, high stability, excellent reuse efficiencies overcoming the costs associated with ligand preparation.

3.4. Frontier molecular orbitals analysis

Frontier Molecular orbitals (FMO), namely Highest Occupied Molecular Orbital (HOMO) and Lowest Unoccupied Molecular Orbital (LUMO) can give important information about the reactivity of different chemical systems; in general a high reactivity is associated to molecules with smaller energy gap between both FMO [ΔE (HOMO-LUMO)] [114–116]. Fig. 14a shows a HOMO-LUMO plot of **Si3PyS** and **Si4PyS** and the calculated energies. By analyzing the HOMO→LUMO transition in terms of electron density is noticeable, that for **Si3PyS,** this transition involves a charge transfer from and to the same pyrrolic type rings, while for **Si4PyS**, the electronic charge transfer occurs from the extra substituted trifluorophenyl unit to the pyrrole-type units. The energy gaps of **Si3PyS** and **Si4PyS** are close to each other (2.252 eV and 2.193 eV respectively) although the slightly lower gap for **Si4PyS** agrees with its, in general, somewhat better extraction capability towards the metal ions (Cu^{2+}, Pb^{2+} and Cd^{2+}).

3.5. Molecular electrostatic potential (MESP) minima analysis

Molecular electrostatic potential (MESP) is a very useful descriptor for predicting chemical reactive sites. Quantitative analysis of the molecular surface shows the extreme points of the electrostatic potential, known as local minima and maxima points, which indicate the nucleophilic (electron-rich) and electrophilic (electron-poor) sites of a molecule. Fig. 14b and c shows the local minima points calculated for **Si3PyS** and **Si4PyS,** after a geometric optimization by DFT using the B3LYP-6–31 G(d,p) method, as green spheres with the corresponding calculated values. As expected, both hybrids show the presence of two minima points located at the inner of the porphyrinic cavity formed by the four-coordinating nitrogen of the pyrrole-type units with the values of (−78.96 and −78.82 kcal mol^{-1}) and (−76.54 and −76.81 kcal mol^{-1}) for **Si3PyS** and **Si4PyS** respectively. The distances separating these minima from the *N*-pyrrole units have been calculated and show values ranging from 2.06 Å and 2.20 Å (see Fig. 14d); these values represent the approximate lengths of the coordination bonds and are more suitable for Cu^{2+} than for Pb^{2+} which has a longer ionic radius. Interesting, the other minima surrounding the structure of the studied materials have a symmetrical distribution of values for **Si4PyS** (−34.57, −35.10, −36.76 and −34.51 kcal mol^{-1}) and non-symmetrical distribution values for **Si3PyS** (−35.45, −35.10, −34.88 and −10.38 ∼ −13.94 kcal mol^{-1}). This can be a symptom of the higher stability of the metallic complexes formed by **Si4PyS** and can explain its slightly improved extractive efficiency towards Cu^{2+} when compared to the **Si3PyS** hybrid. In addition, the electron-rich sites around the structure of the studied materials can explain the much better efficiency of both hybrids when compared with the starting scaffold 5,10,15,20-tetrakis(pentafluorophenyl)porphyrin**.** The other points not represented have low enough energies to attract the electronic clouds towards it.

4. Conclusions

The new hybrids **Si3PyS** and **Si4PyS** constituted by functionalized silica gel covalently linked to highly chelating porphyrins have been successfully synthesized via a simple heterogeneous procedure. Their characterization using adequate techniques confirmed the structural integrity and the preservation of the mesoporous structure of **Si** after the covalent attachment of the porphyrins. The two new adsorbents displayed excellent adsorption capacities towards Cu^{2+}, Pb^{2+}, Zn^{2+} and Cd^{2+} compared to several reported sorbents. The highest adsorption capacities of the sorbents **Si3PyS** and **Si4PyS** were observed for Cu^{2+} attaining values of 176.32 mg g^{-1} and 184.15 mg g^{-1}, respectively. A pH of 6 is the optimal pH for the maximum uptake of metal ions. In addition, the adsorption equilibrium can be reached up to 15 min, suggesting rapid external diffusion and surface adsorption. The adsorption kinetics fit into the pseudo-second-order model and shows the homogeneous characteristics. The comparison of different isotherm models indicated that the Langmuir model gave the best fit to the experimental data. The thermodynamic parameters agree with an endothermic and spontaneous process. These materials present a high selectivity for Cu^{2+} compared to other metal ions and their application for the extraction of metals from natural waters (Moulouya Rivers) and industrial wastewater (Industrial zone of Oujda, Morocco) was reliable. The adsorbents can be regenerated several times without loss of organic moiety on the surface of silica gel and without losing their remarkable efficiency in the removal of metal cations. Thus, it can be concluded that **Si3PyS** and **Si4PyS** are an effective, alternative, and low-cost adsorbents synthons for the quantitative removal of heavy metals, especially Cu^{2+}, from aqueous solutions and wastewater. DFT calculations carried out clearly explain the enhanced reactivity of **Si4PyS** for the extraction of metal cations.

Funding

This research was funded by FCT/MCT (Fundação para a Ciência e Tecnologia and Ministério da Ciência, Tecnologia e Ensino Superior) through the financial support to LAQV-REQUIMTE (UIDB/50006/2020 and UIDP/50006/2020) CICECO – Aveiro Institute of Materials (UIDB/50011/2020 & UIDP/50011/2020) and to project PORP2PS(EXPL/QUI-QOR/0586/2021), through national funds and, when applicable, co-financed by the FEDER, within the PT2020 Partnership Agreement. NMM Moura and F Figueira thanks FCT (Fundação para a Ciência e Tecnologia) for funding through program DL 57/2016 – Norma transitória (CDL-CTTRI-048-88-ARH/2018 and CDL-CTTRI-168-89-ARH/2018, respectively). The authors extend their appreciation to the PPR2-

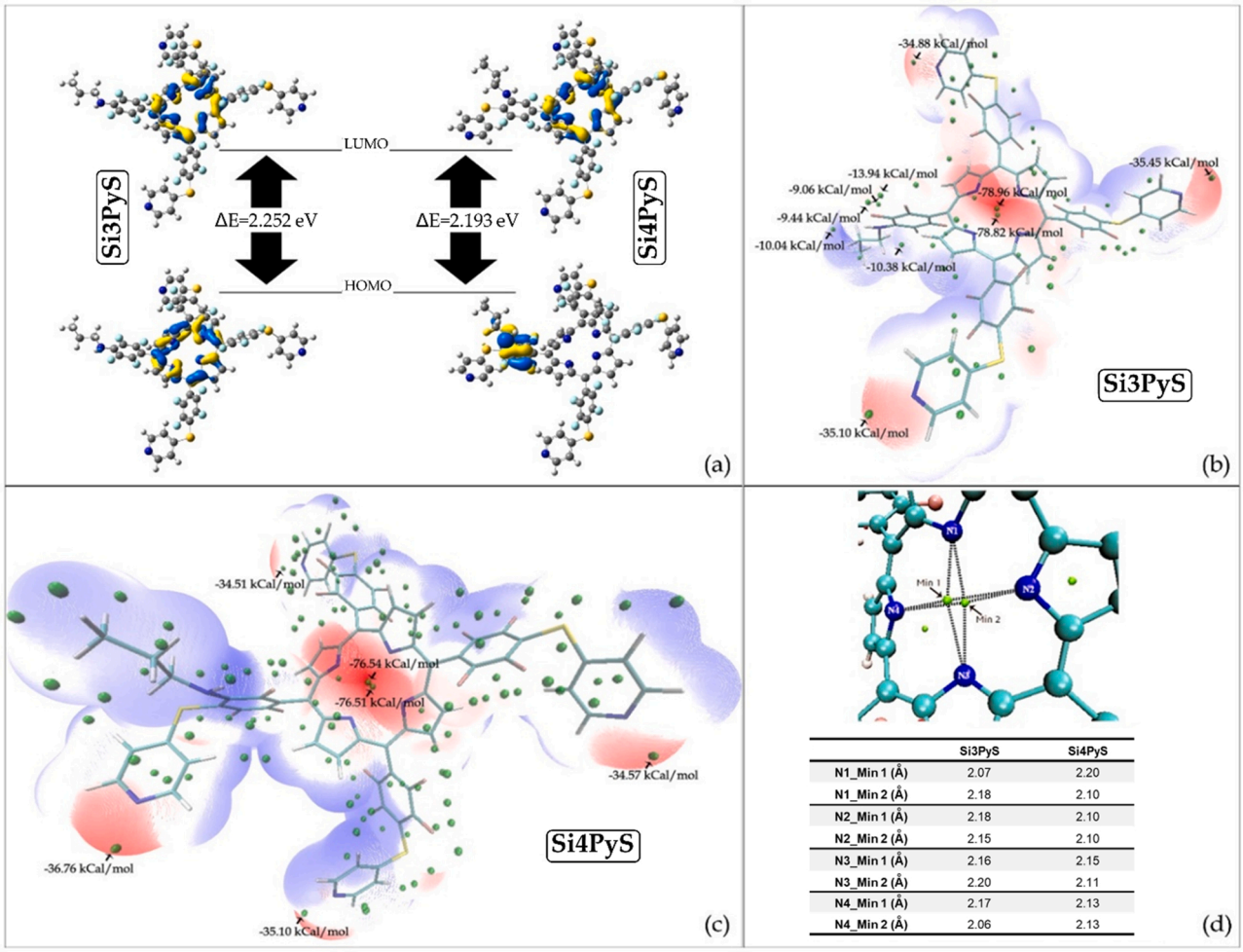

	Si3PyS	Si4PyS
N1_Min 1 (Å)	2.07	2.20
N1_Min 2 (Å)	2.18	2.10
N2_Min 1 (Å)	2.18	2.10
N2_Min 2 (Å)	2.15	2.10
N3_Min 1 (Å)	2.16	2.15
N3_Min 2 (Å)	2.20	2.11
N4_Min 1 (Å)	2.17	2.13
N4_Min 2 (Å)	2.06	2.13

Fig. 14. (a) HOMO-LUMO Shapes of **Si3PyS** and **Si4PyS**; (b and c) Minima points of MESP of **Si3PyS** and **Si4PyS**; (d) Distances separating minima points from *N*-azole.

MESRSFC-CNRST-P10 project (Morocco) for the financial support.

CRediT authorship contribution statement

Chahrazad El Abiad: Investigation, Writing – original draft. **Smaail Radi**: Conceptualization, Writing – review & editing, Supervision. **Mohamed El Massaoudi**: Methodology, Formal analysis, Writing – review & editing. **Morad Lamsayah**: Investigation, Writing – original draft. **Flávio Figueira**: Investigation, Formal analysis, Writing – review & editing. **Maria A. F. Faustino**: Validation, Writing – review & editing **M. Graça P.M.S. Neves**: Writing – review & editing, Supervision. **Nuno M.M. Moura**: Investigation, Methodology, Formal analysis, Writing – review & editing.

Declaration of Competing Interest

The authors declare that they have no known competing financial interests or personal relationships that could have appeared to influence the work reported in this paper.

Data availability

Data will be made available on request.

Acknowledgments

The authors acknowledge to University of Aveiro, to FCT/MCTES, and to the Portuguese NMR Network. NMM Moura and F Figueira thanks FCT (Fundação para a Ciência e Tecnologia) for funding through program DL 57/2016 – Norma transitória (CDL-CTTRI-048-88-ARH/2018 and CDL-CTTRI-168-89-ARH/2018, respectively).

References

[1] L. Rizzo, Addressing main challenges in the tertiary treatment of urban wastewater: are homogeneous photodriven AOPs the answer? Environ. Sci. Water Res. Technol. 8 (2022) 2145–2169, https://doi.org/10.1039/D2EW00146B.
[2] C. Zhao, Y. Wang, X. Wang, D.D. Dionysiou, Treatment of contaminants of emerging concern and pathogens using electrophotocatalytic processes: a review, Curr. Opin. Green Sustain. Chem. 32 (2021), 100527, https://doi.org/10.1016/J.COGSC.2021.100527.
[3] L. Rizzo, S. Malato, D. Antakyali, V.G. Beretsou, M.B. Đolić, W. Gernjak, E. Heath, I. Ivancev-Tumbas, P. Karaolia, A.R. Lado Ribeiro, G. Mascolo, C.S. McArdell, H. Schaar, A.M.T. Silva, D. Fatta-Kassinos, Consolidated vs new advanced treatment methods for the removal of contaminants of emerging concern from urban wastewater, Sci. Total Environ. 655 (2019) 986–1008, https://doi.org/10.1016/J.SCITOTENV.2018.11.265.
[4] L. Joseph, B.M. Jun, M. Jang, C.M. Park, J.C. Muñoz-Senmache, A.J. Hernández-Maldonado, A. Heyden, M. Yu, Y. Yoon, Removal of contaminants of emerging concern by metal-organic framework nanoadsorbents: a review, Chem. Eng. J. 369 (2019) 928–946, https://doi.org/10.1016/J.CEJ.2019.03.173.
[5] M. Bartolomeu, M.G.P.M.S. Neves, M.A.F. Faustino, A. Almeida, Wastewater chemical contaminants: remediation by advanced oxidation processes, Photochem. Photobiol. Sci. 17 (2018) 1573–1598, https://doi.org/10.1039/C8PP00249E.

[6] F. Suhail, M. Batool, M.I. Din, M.A. Khan, G.A. Chotana, I. Zubair, A.T. Shah, Facile synthesis of hetaryl-modified MCM-41 and targeted removal of Pb(II) ions for water purification, J. Porous Mater. 27 (2020) 1491–1504, https://doi.org/10.1007/s10934-020-00919-8.
[7] A. Dolgormaa, C.-J. Lv, Y. Li, J. Yang, J.-X. Yang, P. Chen, H.-P. Wang, J. Huang, Adsorption of Cu(II) and Zn(II) ions from aqueous solution by Gel/PVA-modified super-paramagnetic iron oxide nanoparticles, Molecules 23 (2018) 2982, https://doi.org/10.3390/molecules23112982.
[8] R. Kumar, M.A. Laskar, I.F. Hewaidy, M.A. Barakat, Modified adsorbents for removal of heavy metals from aqueous environment: a review, Earth Syst. Environ. 3 (2019) 83–93, https://doi.org/10.1007/s41748-018-0085-3.
[9] X.-X. Liang, N. Wang, Y.-L. Qu, L.-Y. Yang, Y.-G. Wang, X.-K. Ouyang, Facile preparation of metal-organic framework (MIL-125)/chitosan beads for adsorption of Pb(II) from aqueous solutions, Molecules 23 (2018) 1524, https://doi.org/10.3390/molecules23071524.
[10] A.S. Mohammed, A. Kapri, R. Goel, Heavy metal pollution: source, impact, and remedies, Environ. Pollut. (2011) 1–28, https://doi.org/10.1007/978-94-007-1914-9_1.
[11] Y. Liu, H. Wang, Y. Cui, N. Chen, Removal of copper ions from wastewater: a review, Int. J. Environ. Res. Public Health 20 (2023) 3885, https://doi.org/10.3390/IJERPH20053885.
[12] M. Mohsen-Nia, P. Montazeri, H. Modarress, Removal of Cu2+ and Ni2+ from wastewater with a chelating agent and reverse osmosis processes, Desalination 217 (2007) 276–281, https://doi.org/10.1016/j.desal.2006.01.043.
[13] J. Rubio, M.L. Souza, R.W. Smith, Overview of flotation as a wastewater treatment technique, Miner. Eng. 15 (2002) 139–155, https://doi.org/10.1016/s0892-6875(01)00216-3.
[14] Z. Wu, M. He, X. Guo, R. Zhou, Removal of antimony (III) and antimony (V) from drinking water by ferric chloride coagulation: competing ion effect and the mechanism analysis, Sep. Purif. Technol. 76 (2010) 184–190, https://doi.org/10.1016/j.seppur.2010.10.006.
[15] A. Wójtowicz, A. Stokłosa, Removal of heavy metal ions on smectite ion-exchange column, Polish J. Environ. Stud., 11, n.d., pp. 97–101. ⟨http://www.pjoes.com/Removal-of-Heavy-Metal-Ions-on-Smectite-Ion-Exchange-Column,87428,0,2.html⟩ (Accessed 5 September 2022).
[16] Y. Ku, I.-L. Jung, Photocatalytic reduction of Cr(VI) in aqueous solutions by UV irradiation with the presence of titanium dioxide, Water Res. 35 (2001) 135–142, https://doi.org/10.1016/s0043-1354(00)00098-1.
[17] H. Bessbousse, T. Rhlalou, J.-F. Verchère, L. Lebrun, Sorption and filtration of Hg (II) ions from aqueous solutions with a membrane containing poly (ethyleneimine) as a complexing polymer, J. Membr. Sci. 325 (2008) 997–1006, https://doi.org/10.1016/j.memsci.2008.09.035.
[18] A. Ahmad, S.H. Mohd-Setapar, C.S. Chuong, A. Khatoon, W.A. Wani, R. Kumar, M. Rafatullah, Recent advances in new generation dye removal technologies: novel search for approaches to reprocess wastewater, RSC Adv. 5 (2015) 30801–30818, https://doi.org/10.1039/c4ra16959j.
[19] M. Neznakomova, S. Boteva, L. Tzankov, M. Elhag, Non-woven textile materials from waste fibers for cleanup of waters polluted with petroleum and oil products, Earth Syst. Environ. 2 (2018) 413–420, https://doi.org/10.1007/s41748-018-0048-8.
[20] W.S. Wan Ngah, L.C. Teong, M.A.K.M. Hanafiah, Adsorption of dyes and heavy metal ions by chitosan composites: a review, Carbohydr. Polym. 83 (2011) 1446–1456, https://doi.org/10.1016/j.carbpol.2010.11.004.
[21] S. Mondal, S. Chatterjee, S. Mondal, A. Bhaumik, Thioether-functionalized covalent triazine nanospheres: a robust adsorbent for mercury removal, ACS Sustain. Chem. Eng. 7 (2019) 7353–7361, https://doi.org/10.1021/acssuschemeng.9b00567.
[22] S. Nayab, H. Baig, A. Ghaffar, E. Tuncel, Z. Oluz, H. Duran, B. Yameen, Silica based inorganic-organic hybrid materials for the adsorptive removal of chromium, RSC Adv. 8 (2018) 23963–23972, https://doi.org/10.1039/c8ra04209h.
[23] A. Beveridge, W.F. Pickering, The influence of surfactants on the adsorption of heavy metal ions by clays, Water Res. 17 (1983) 215–225, https://doi.org/10.1016/0043-1354(83)90102-1.
[24] M. Machida, Y. Amano, M. Aikawa, Adsorptive removal of heavy metal ions by activated carbons, Carbon 49 (2011) 3393, https://doi.org/10.1016/j.carbon.2011.04.011.
[25] Z. Wang, K. Tan, J. Cai, S. Hou, Y. Wang, P. Jiang, M. Liang, Silica oxide encapsulated natural zeolite for high efficiency removal of low concentration heavy metals in water, Colloids Surf. A Physicochem. Eng. Asp. 561 (2019) 388–394, https://doi.org/10.1016/j.colsurfa.2018.10.065.
[26] G. Feng, J. Ma, X. Zhang, Q. Zhang, Y. Xiao, Q. Ma, S. Wang, Magnetic natural composite Fe3O4-chitosan@bentonite for removal of heavy metals from acid mine drainage, J. Colloid Interface Sci. 538 (2019) 132–141, https://doi.org/10.1016/j.jcis.2018.11.087.
[27] B. Ramalingam, T. Parandhaman, P. Choudhary, S.K. Das, Biomaterial functionalized graphene-magnetite nanocomposite: a novel approach for simultaneous removal of anionic dyes and heavy-metal ions, ACS Sustain. Chem. Eng. 6 (2018) 6328–6341, https://doi.org/10.1021/acssuschemeng.8b00139.
[28] M. d'Halluin, J. Rull-Barrull, G. Bretel, C. Labrugère, E. Le Grognec, F.-X. Felpin, Chemically modified cellulose filter paper for heavy metal remediation in water, ACS Sustain. Chem. Eng. 5 (2017) 1965–1973, https://doi.org/10.1021/acssuschemeng.6b02768.
[29] S. Wu, F. Li, R. Xu, S. Wei, G. Li, Synthesis of thiol-functionalized MCM-41 mesoporous silicas and its application in Cu(II), Pb(II), Ag(I), and Cr(III) removal, J. Nanopart. Res. 12 (2009) 2111–2124, https://doi.org/10.1007/s11051-009-9770-3.
[30] S. Wongsakulphasatch, W. Kiatkittipong, J. Saiswat, B. Oonkhanond, A. Striolo, S. Assabumrungrat, The adsorption aspect of Cu2+ and Zn2+ on MCM-41 and SDS-modified MCM-41, Inorg. Chem. Commun. 46 (2014) 301–304, https://doi.org/10.1016/j.inoche.2014.06.029.
[31] T. Zhou, X. Cheng, Y. Pan, C. Li, L. Gong, H. Zhang, Mechanical performance and thermal stability of glass fiber reinforced silica aerogel composites based on co-precursor method by freeze drying, Appl. Surf. Sci. 437 (2018) 321–328, https://doi.org/10.1016/j.apsusc.2017.12.146.
[32] S. Alasti Bonab, J. Moghaddas, M. Rezaei, In-situ synthesis of silica aerogel/polyurethane inorganic-organic hybrid nanocomposite foams: characterization, cell microstructure and mechanical properties, Polymer 172 (2019) 27–40, https://doi.org/10.1016/j.polymer.2019.03.050.
[33] I. Osica, G. Imamura, K. Shiba, Q. Ji, L.K. Shrestha, J.P. Hill, K.J. Kurzydłowski, G. Yoshikawa, K. Ariga, Highly networked capsular silica–porphyrin hybrid nanostructures as efficient materials for acetone vapor sensing, ACS Appl. Mater. Interfaces 9 (2017) 9945–9954, https://doi.org/10.1021/acsami.6b15680.
[34] S. Radi, C. El Abiad, N.M.M. Moura, M.A.F. Faustino, M.G.P.M.S. Neves, New hybrid adsorbent based on porphyrin functionalized silica for heavy metals removal: synthesis, characterization, isotherms, kinetics and thermodynamics studies, J. Hazard. Mater. 370 (2019) 80–90, https://doi.org/10.1016/j.jhazmat.2017.10.058.
[35] C.M.B. Neves, S.L.H. Rebelo, M.A.F. Faustino, M.G.P.M.S. Neves, M.M.Q. Simões, Second-generation manganese(III) porphyrins bearing 3,5-dichloropyridyl units: Innovative homogeneous and heterogeneous catalysts for the epoxidation of alkenes, Catalysts 9 (2019) 967, https://doi.org/10.3390/catal9110967.
[36] D. Zhao, Y. Wang, Y. Xu, N. Wang, J. Li, Preparation, characterization and catalytic oxidation properties of silica composites immobilized with cationic metalloporphyrins, J. Mater. Sci. 53 (2018) 14241–14249, https://doi.org/10.1007/s10853-018-2662-0.
[37] K.A.D.F. Castro, M. Halma, G.S. Machado, G.P. Ricci, G.M. Ucoski, K.J. Ciuffi, S. Nakagaki, Preparation of catalysts based on iron(III) porphyrins heterogenized on silica obtained by the Sol-Gel process for hydroxylation and epoxidation reactions, J. Braz. Chem. Soc. 21 (2010) 1329–1340, https://doi.org/10.1590/s0103-50532010000700020.
[38] I. Sebarchievici, B.-O. Taranu, S.F. Rus, E. Fagadar-Cosma, Electrochemical behaviour and analytical applications of a manganese porphyrin – silica hybrid film prepared by pulsed laser deposition, J. Electroanal. Chem. 865 (2020), 114127, https://doi.org/10.1016/j.jelechem.2020.114127.
[39] M. Pawlaczyk, G. Schroeder, Adsorption studies of Cu(II) ions on dendrimer-grafted silica-based materials, J. Mol. Liq. 281 (2019) 176–185, https://doi.org/10.1016/j.molliq.2019.02.043.
[40] B. Ren, K. Wang, B. Zhang, H. Li, Y. Niu, H. Chen, Z. Yang, X. Li, H. Zhang, Adsorption behavior of PAMAM dendrimers functionalized silica for Cd(II) from aqueous solution: experimental and theoretical calculation, J. Taiwan Inst. Chem. Eng. 101 (2019) 80–91, https://doi.org/10.1016/j.jtice.2019.04.037.
[41] W. Shan, D. Wang, Z. Zhang, Z. Lou, Y. Xiong, Y. Fan, Synthesis of Schiff base-functionalized silica for effective adsorption of Re(VII) from aqueous solution, J. Taiwan Inst. Chem. Eng. 100 (2019) 277–284, https://doi.org/10.1016/j.jtice.2019.04.025.
[42] M. El-Massaoudi, S. Radi, M. Bacquet, S. Degoutin, Y. Garcia, Highly efficient and selective adsorbent for potentially toxic metals removal from aquatic media, J. Environ. Chem. Eng. 6 (2018) 5980–5989, https://doi.org/10.1016/j.jece.2018.09.010.
[43] J. Deng, H. Li, M. Yang, F. Wu, Palladium porphyrin complexes for photodynamic cancer therapy: effect of porphyrin units and metal, Photochem. Photobiol. Sci. 19 (2020) 905–912, https://doi.org/10.1039/c9pp00363k.
[44] S.D. Gokakakar, P.A. Pavaskar, A.V. Salker, Photo-catalytic studies of Mn and Fe tetraphenyl porphyrins in the degradation of Amido Black 10B dye with solar light, SN Appl. Sci. 2 (2020) 294, https://doi.org/10.1007/s42452-020-1989-8.
[45] C. Di Natale, D. Monti, R. Paolesse, Chemical sensitivity of porphyrin assemblies, Mater. Today 13 (2010) 46–52, https://doi.org/10.1016/s1369-7021(10)70127-9.
[46] K.M. Kadish, K.M. Smith, R. Guilard, With applications to chemistry, physics, materials science, engineering, biology and medicine, in: Handbook of Porphyrin Science, World Scientific Publishing Company, 2016, https://doi.org/10.1142/10055-vol40.
[47] F. Figueira, J.M.M. Rodrigues, A.A.S. Farinha, J.A.S. Cavaleiro, J.P.C. Tomé, Synthesis and anion binding properties of porphyrins and related compounds, J. Porphyr. Phthalocyanines 20 (2016) 950–965, https://doi.org/10.1142/s1088424616300135.
[48] D. Anghel, A. Lascu, C. Epuran, I. Fratilescu, C. Ianasi, M. Birdeanu, E. Fagadar-Cosma, Hybrid materials based on silica matrices impregnated with Pt-porphyrin or PtNPs destined for CO(2) gas detection or for wastewaters color removal, Int. J. Mol. Sci. 21 (2020) 4262, https://doi.org/10.3390/ijms21124262.
[49] F. Figueira, J.A.S. Cavaleiro, J.P.C. Tomé, Silica nanoparticles functionalized with porphyrins and analogs for biomedical studies, J. Porphyr. Phthalocyanines 15 (2011) 517–533, https://doi.org/10.1142/s1088424611003653.
[50] M. De Carluccio, A. Fiorentino, L. Rizzo, Multi-barrier treatment of mature landfill leachate: effect of Fenton oxidation and air stripping on activated sludge process and cost analysis, J. Environ. Chem. Eng. 8 (2020), 104444, https://doi.org/10.1016/J.JECE.2020.104444.
[51] Y. Li, Y. Yang, J. Lei, W. Liu, M. Tong, J. Liang, The degradation pathways of carbamazepine in advanced oxidation process: a mini review coupled with DFT

calculation, Sci. Total Environ. 779 (2021), 146498, https://doi.org/10.1016/j.scitotenv.2021.146498.
[52] V.A. Adole, T.B. Pawar, B.S. Jagdale, DFT computational insights into structural, electronic and spectroscopic parameters of 2-(2-Hydrazineyl)thiazole derivatives: a concise theoretical and experimental approach, J. Sulfur Chem. 42 (2020) 131–148, https://doi.org/10.1080/17415993.2020.1817456.
[53] B. Hashemzadeh, L. Edjlali, P.D. Kheirollahi Nezhad, E. Vessally, Hexa-cata-hexabenzocoronene nanographene as a promising anode material for Mg-ion batteries, J. Mol. Model. 27 (2021), https://doi.org/10.1007/s00894-021-04675-7.
[54] Y. Ding, G. Wang, F. Sun, Y. Lin, Heterogeneous nanostructure design based on the epitaxial growth of spongy MoSx on 2D Co(OH)2 nanoflakes for triple-enzyme mimetic activity: experimental and density functional theory studies on the dramatic activation mechani, ACS Appl. Mater. Interfaces 10 (2018) 32567–32578, https://doi.org/10.1021/acsami.8b10560.
[55] R. Kavitha, S. Nirmala, R. Nithyabalaji, R. Sribalan, Biological evaluation, molecular docking and DFT studies of charge transfer complexes of quinaldic acid with heterocyclic carboxylic acid, J. Mol. Struct. 1204 (2020), 127508, https://doi.org/10.1016/j.molstruc.2019.127508.
[56] A. Halal, K.S. Rahman, S.F. Abdullah, K. Sopian, N. Amin, An investigation on CdS1-xTex interface compound in CdS/CdTe hetero-junction solar cells by density functional theory (DFT), Superlattices Microstruct. 151 (2021), 106805, https://doi.org/10.1016/j.spmi.2021.106805.
[57] M. Haroon, A.A. Al-Saadi, M.R.S.A. Janjua, Insights into end-capped modifications effect on the photovoltaic and optoelectronic properties of S-shaped fullerene-free acceptor molecules: a density functional theory computational study for organic solar cells, J. Phys. Org. Chem. 35 (2022), https://doi.org/10.1002/poc.4314.
[58] K.C. Bhamu, A. Soni, J. Sahariya, Revealing optoelectronic and transport properties of potential perovskites Cs2PdX6 (X = Cl, Br): a probe from density functional theory (DFT, Sol. Energy 162 (2018) 336–343, https://doi.org/10.1016/j.solener.2018.01.059.
[59] S. Kamaal, M. Usman, M. Afzal, A. Alarifi, A. Ali, R. Das, P. Lama, M. Ahmad, A new copper(II)-based layered coordination polymer: crystal structure, topology, QTAIM analysis, experimental and theoretical magnetic properties based on DFT combined with broken-symmetry formalism (BS-DFT), Polyhedron 193 (2021), 114881, https://doi.org/10.1016/j.poly.2020.114881.
[60] R. Pettinari, F. Marchetti, A. Tombesi, C. Di Nicola, C. Pettinari, C. Guo, Z. Zhang, A. Galindo, F. Fadaei-Tirani, M. Hadiji, P.J. Dyson, Arene-ruthenium(II) complexes with pyrazole-based ligands bearing a pyridine moiety: synthesis, structure, DFT calculations, and cytotoxicity, Inorg. Chim. Acta 528 (2021), 120610, https://doi.org/10.1016/j.ica.2021.120610.
[61] R. Fouad, I.A. Shaaban, T.E. Ali, M.A. Assiri, S.S. Shenouda, Co(ii), Ni(ii), Cu(ii) and Cd(ii)-thiocarbonohydrazone complexes: spectroscopic, DFT, thermal, and electrical conductivity studies, RSC Adv. 11 (2021) 37726–37743, https://doi.org/10.1039/d1ra06902k.
[62] S.E. Korolenko, K.P. Zhuravlev, V.I. Tsaryuk, A.S. Kubasov, V.V. Avdeeva, EA Malinina, A.S. Burlov, L.N. Divaeva, K.Y. Zhizhin, N.T. Kuznetsov, Crystal structures, luminescence, and DFT study of mixed-ligand Zn(II) and Cd(II) complexes with phenyl-containing benzimidazole derivatives with linker C N or N N group, J. Lumin. 237 (2021), 118156, https://doi.org/10.1016/j.jlumin.2021.118156.
[63] R. Soury, M. Chaabene, M. Jabli, Y. Rousselin, Synthesis, characterization, and computational study of a new zinc derivative (4.4′diaminodiphenylmethane) (meso-tetratolylporphyrinato) zinc {[Zn(TTP) (DADMP)2]}n, J. Solid State Chem. 295 (2021), 121920, https://doi.org/10.1016/J.JSSC.2020.121920.
[64] B. Chilukuri, U. Mazur, K.W. Hipps, Structure, properties, and reactivity of porphyrins on surfaces and nanostructures with periodic DFT calculations, Appl. Sci. 10 (2020) 740, https://doi.org/10.3390/APP10030740.
[65] J. Schindler, S. Kupfer, A.A. Ryan, K.J. Flanagan, M.O. Senge, B. Dietzek, Sterically induced distortions of nickel(II) porphyrins – comprehensive investigation by DFT calculations and resonance Raman spectroscopy, Coord. Chem. Rev. 360 (2018) 1–16, https://doi.org/10.1016/J.CCR.2017.12.014.
[66] J.P. Janet, Q. Zhao, E.I. Ioannidis, H.J. Kulik, Density functional theory for modelling large molecular adsorbate–surface interactions: a mini-review and worked example, Mol. Simul. 43 (2016) 327–345, https://doi.org/10.1080/08927022.2016.1258465.
[67] A.K. Mandal, M. Taniguchi, J.R. Diers, D.M. Niedzwiedzki, C. Kirmaier, J. S. Lindsey, D.F. Bocian, D. Holten, Photophysical properties and electronic structure of porphyrins bearing zero to four meso-phenyl substituents: new insights into seemingly well understood tetrapyrroles, J. Phys. Chem. A 120 (2016) 9719–9731, https://doi.org/10.1021/ACS.JPCA.6B09483/ASSET/IMAGES/LARGE/JP-2016-094836_0014.JPEG.
[68] M.C. Gomes, S.M. Woranovicz-Barreira, M.A.F. Faustino, R. Fernandes, M.G.P.M. S. Neves, A.C. Tomé, N.C.M. Gomes, A. Almeida, J.A.S. Cavaleiro, Â. Cunha, J.P. C. Tomé, Photodynamic inactivation of Penicillium chrysogenum conidia by cationic porphyrins, Photochem. Photobiol. Sci. 10 (2011) 1735–1743, https://doi.org/10.1039/c1pp05174a.
[69] K.A.D.F. Castro, F. Figueira, R.F. Mendes, F.A. Almeida Paz, M. da, G.P.M. S. Neves, J.A.S. Cavaleiro, S. Nakagaki, J.P.C. Tomé, M.M.Q. Simões, Porphyrinic coordination polymer-type materials as heterogeneous catalysts in catechol oxidation, Polyhedron 158 (2019) 478–484, https://doi.org/10.1016/j.poly.2018.11.022.
[70] K.A.D.F. Castro, F. Figueira, R.F. Mendes, J.A.S. Cavaleiro, M.G.P.M.S. Neves, M. M.Q. Simões, F.A. A. Paz, J.P.C. Tomé, S. Nakagaki, Copper–porphyrin–metal–organic frameworks as oxidative heterogeneous catalysts, ChemCatChem 9 (2017) 2939–2945, https://doi.org/10.1002/cctc.201700484.
[71] C.P.S. Ribeiro, S.R.D. Gamelas, M.A.F. Faustino, A.T.P.C. Gomes, J.P.C. Tomé, A. Almeida, L.M.O. Lourenço, Unsymmetrical cationic porphyrin-cyclodextrin bioconjugates for photoinactivation of Escherichia coli, Photodiagn. Photodyn. Ther. 31 (2020), 101788, https://doi.org/10.1016/j.pdpdt.2020.101788.
[72] S. Radi, C. El Abiad, A.P. Carvalho, S.M. Santos, M.A.F. Faustino, M.G.P.M. S. Neves, N.M.M. Moura, An efficient hybrid adsorbent based on silica-supported amino penta-carboxylic acid for water purification, J. Mater. Chem. A 6 (2018), https://doi.org/10.1039/c8ta02560f.
[73] O. Frisch, M.J. Trucks, G.W. Schlegel, H.B. Scuseria, G.E. Robb, M.A. Cheeseman, J.R. Scalmani, G. Barone, V. Mennucci, B. Petersson, G.A. Nakatsuji, H. Caricato, M. Li, X. Hratchian, H.P. Izmaylov, A.F. Bloino, J. Zheng, G. Sonnenb. Gaussian 09, Revision E01, 2009, pp. 20–44 (Accessed 5 September 2022), ⟨https://gaussian.com/g09citation/⟩.
[74] A.D. Becke, Density-functional exchange-energy approximation with correct asymptotic behavior, Phys. Rev. A 38 (1988) 3098–3100, https://doi.org/10.1103/physreva.38.3098.
[75] V.A. Rassolov, M.A. Ratner, J.A. Pople, P.C. Redfern, L.A. Curtiss, 6–31G* basis set for third-row atoms, J. Comput. Chem. 22 (2001) 976–984, https://doi.org/10.1002/jcc.1058.
[76] T. Lu, F. Chen, Multiwfn: a multifunctional wavefunction analyzer, J. Comput. Chem. 33 (2011) 580–592, https://doi.org/10.1002/jcc.22885.
[77] W. Humphrey, A. Dalke, K. Schulten, VMD: visual molecular dynamics, J. Mol. Graph. 14 (1996) 33–38, https://doi.org/10.1016/0263-7855(96)00018-5.
[78] J.I.T. Costa, A.C. Tomé, M.G.P.M.S. Neves, J.A.S. Cavaleiro, 5,10,15,20-tetrakis (pentafluorophenyl)porphyrin: a versatile platform to novel porphyrinic materials, J. Porphyr. Phthalocyanines 15 (2011) 1116–1133, https://doi.org/10.1142/S1088424611004294.
[79] G.E. Berendsen, L. de Galan, Preparation and chromatographic properties of some chemically bonded phases for reversed-phase liquid chromatography, J. Liq. Chromatogr. 1 (2006) 561–586, https://doi.org/10.1080/01483917808060019.
[80] R. Mutneja, R. Singh, V. Kaur, J. Wagler, S. Fels, E. Kroke, Schiff base tailed silatranes for the fabrication of functionalized silica based magnetic nano-cores possessing active sites for the adsorption of copper ions, New J. Chem. 40 (2016) 1640–1648, https://doi.org/10.1039/c5nj02287h.
[81] S. Brunauer, P.H. Emmett, E. Teller, Adsorption of gases in multimolecular layers, J. Am. Chem. Soc. 60 (1938) 309–319, https://doi.org/10.1021/ja01269a023.
[82] M. Machida, B. Fotoohi, Y. Amamo, T. Ohba, H. Kanoh, L. Mercier, Cadmium(II) adsorption using functional mesoporous silica and activated carbon, J. Hazard. Mater. 221–222 (2012) 220–227, https://doi.org/10.1016/j.jhazmat.2012.04.039.
[83] C.E. Abiad, S. Radi, M.A.F. Faustino, M.P.M.S. Graça Neves, N.M.M. Moura, Supramolecular hybrid material based on engineering porphyrin hosts for an efficient elimination of lead(II) from aquatic medium, Molecules 24 (2019) 669, https://doi.org/10.3390/molecules24040669.
[84] J.A.A. Sales, C. Airoldi, Calorimetric investigation of metal ion adsorption on 3-glycidoxypropyltrimethylsiloxane + propane-1,3-diamine immobilized on silica gel, Thermochim. Acta 427 (2005) 77–83, https://doi.org/10.1016/j.tca.2004.08.015.
[85] J.A.A. Sales, F.P. Faria, A.G.S. Prado, C. Airoldi, Attachment of 2-aminomethyl-pyridine molecule onto grafted silica gel surface and its ability in chelating cations, Polyhedron 23 (2004) 719–725, https://doi.org/10.1016/j.poly.2003.11.051.
[86] Y. Tian, P. Yin, R. Qu, C. Wang, H. Zheng, Z. Yu, Removal of transition metal ions from aqueous solutions by adsorption using a novel hybrid material silica gel chemically modified by triethylenetetraminomethylenephosphonic acid, Chem. Eng. J. 162 (2010) 573–579, https://doi.org/10.1016/j.cej.2010.05.065.
[87] A.E. Regazzoni, Adsorption kinetics at solid/aqueous solution interfaces: on the boundaries of the pseudo-second order rate equation, Colloids Surf. A Physicochem. Eng. Asp. 585 (2020), 124093, https://doi.org/10.1016/j.colsurfa.2019.124093.
[88] J. Bujdák, Adsorption kinetics models in clay systems. The critical analysis of pseudo-second order mechanism, Appl. Clay Sci. 191 (2020), 105630, https://doi.org/10.1016/j.clay.2020.105630.
[89] L. Largitte, R. Pasquier, A review of the kinetics adsorption models and their application to the adsorption of lead by an activated carbon, Chem. Eng. Res. Des. 109 (2016) 495–504, https://doi.org/10.1016/j.cherd.2016.02.006.
[90] Y. Xiao, J. Azaiez, J.M. Hill, Erroneous application of pseudo-second-order adsorption kinetics model: ignored assumptions and spurious correlations, Ind. Eng. Chem. Res. 57 (2018) 2705–2709, https://doi.org/10.1021/acs.iecr.7b04724.
[91] H. Li, D. Xi, Y. Niu, C. Wang, F. Xu, L. Liang, P. Xu, Design, synthesis and biological evaluation of cobalt(II)-Schiff base complexes as ATP-noncompetitive MEK1 inhibitors, J. Inorg. Biochem. 195 (2019) 174–181, https://doi.org/10.1016/j.jinorgbio.2019.03.022.
[92] Y. Zhou, S. Chen, S. Xi, Z. Wang, P. Deng, F. Yang, Y. Han, Y. Pang, B.Y. Xia, Spatial confinement in copper-porphyrin frameworks enhances carbon dioxide reduction to hydrocarbons, Cell Rep. Phys. Sci. 1 (2020), 100182, https://doi.org/10.1016/j.xcrp.2020.100182.
[93] A.A. Sinelshchikova, S.E. Nefedov, Y.Y. Enakieva, Y.G. Gorbunova, A.Y. Tsivadze, K.M. Kadish, P. Chen, A. Bessmertnykh-Lemeune, C. Stern, R. Guilard, Unusual formation of a stable 2D copper porphyrin network, Inorg. Chem. 52 (2013) 999–1008, https://doi.org/10.1021/ic302257g.
[94] S. Radi, S. Tighadouini, M. Bacquet, S. Degoutin, Y. Garcia, New hybrid material based on a silica-immobilised conjugated β-ketoenol-bipyridine receptor and its

excellent Cu(II) adsorption capacity, Anal. Methods 8 (2016) 6923–6931, https://doi.org/10.1039/c6ay01825d.
[95] S. Tighadouini, S. Radi, M. Ferbinteanu, Y. Garcia, Highly selective removal of Pb (II) by a pyridylpyrazole-β-ketoenol receptor covalently bonded onto the silica surface, ACS Omega 4 (2019) 3954–3964, https://doi.org/10.1021/acsomega.8b03642.
[96] S. Tighadouini, S. Radi, M. Anannaz, M. Bacquet, S. Degoutin, M. Tillard, D. Eddike, H. Amhamdi, Y. Garcia, Engineering β-ketoenol structure functionality in hybrid silica as excellent adsorbent material for removal of heavy metals from water, New J. Chem. 42 (2018) 13229–13240, https://doi.org/10.1039/c8nj01918e.
[97] M. El-Massaoudi, S. Radi, M. Lamsayah, S. Tighadouini, K.K. Séraphin, L. K. Kouassi, Y. Garcia, Ultra-fast and highly efficient hybrid material removes Cu (II) from wastewater: kinetic study and mechanism, J. Clean. Prod. 284 (2021), 124757, https://doi.org/10.1016/j.jclepro.2020.124757.
[98] S. Tighadouini, S. Radi, M. Bacquet, J.-P. Dacquin, Y.N. Mabkhot, S. Jodeh, I. Warad, M. Zaghrioui, Synthesis of 1-(furan-2-yl) imine functionalized silica as a chelating sorbent and its preliminary use in metal ion adsorption, Sep. Sci. Technol. 50 (2014) 710–717, https://doi.org/10.1080/01496395.2014.959134.
[99] K. Robeyns, Y. Garcia, M. Massaoudi, N. Adarsh, A novel environment friendly hybrid material based on a modified silica gel with a bispyrazole derivative for the removal of Zn(II), Pb(II), Cd(II) and Cu(II) traces from aqueous solutions, in: Proceedings of the 6th National Seminar on Crystallography, National Institute of Mental Health and Neuro-Sciences, 2018.
[100] S. Tighadouini, S. Radi, M. Bacquet, S. Degoutin, M. Zaghrioui, S. Jodeh, I. Warad, Removal efficiency of Pb(II), Zn(II), Cd(II) and Cu(II) from aqueous solution and natural water by ketoenol–pyrazole receptor functionalized silica hybrid adsorbent, Sep. Sci. Technol. 52 (2016) 608–621, https://doi.org/10.1080/01496395.2016.1262874.
[101] S. Tighadouini, S. Radi, A. Elidrissi, M. Zaghrioui, Y. Garcia, Selective confinement of Cd ^{II} in silica particles functionalized with β-keto-enol-bisfuran receptor: isotherms, kinetic and thermodynamic studies, Eur. J. Inorg. Chem. 2019 (2019) 3180–3186, https://doi.org/10.1002/ejic.201801349.
[102] S. Tighadouini, S. Radi, A. Elidrissi, K. Haboubi, M. Bacquet, S. Degoutin, M. Zaghrioui, Y. Garcia, Removal of toxic heavy metals from river water samples using a porous silica surface modified with a new β-ketoenolic host, Beilstein J. Nanotechnol. 10 (2019) 262–273, https://doi.org/10.3762/bjnano.10.25.
[103] A. Zhang, L. Gu, K. Hou, C. Dai, C. Song, X. Guo, Mesostructure-tunable and size-controllable hierarchical porous silica nanospheres synthesized by aldehyde-modified Stöber method, RSC Adv. 5 (2015) 58355–58362, https://doi.org/10.1039/c5ra09456a.
[104] Z. Wang, M. Wang, G. Wu, D. Wu, A. Wu, Colorimetric detection of copper and efficient removal of heavy metal ions from water by diamine-functionalized SBA-15, Dalton Trans. 43 (2014) 8461–8468, https://doi.org/10.1039/c3dt53641f.
[105] A. de, O. Jorgetto, A.C.P. da Silva, M.H.P. Wondracek, R.I.V. Silva, E.D. Velini, M. J. Saeki, V.A. Pedrosa, G.R. Castro, Multilayer adsorption of Cu(II) and Cd(II) over Brazilian Orchid Tree (Pata-de-vaca) and its adsorptive properties, Appl. Surf. Sci. 345 (2015) 81–89, https://doi.org/10.1016/j.apsusc.2015.03.142.
[106] A.C.P. Silva, A.O. Jorgetto, M.H.P. Wondracek, M.J. Saeki, J.F. Schneider, V. A. Pedrosa, M.A.U. Martines, G.R. Castro, Characterization of corn (Zea mays) leaf powder and its adsorption properties regarding Cu(II) and Cd(II) from aqueous samples, BioResources 10 (2014), https://doi.org/10.15376/biores.10.1.1099-1114.
[107] S. Pontes Pereira, R. Innocenti Vieira da Silva, M. Juri Saeki, M. Antonio Utrera Martines, V. de Albuquerque Pedrosa, G. Rocha de Castro, A. de Oliveira Jorgetto, Application of mesoporous SBA-15 silica functionalized with 4-amino-2-mercaptopyrimidine for the adsorption of Cu(II), Zn(II), Cd(II), Ni(II) and Pb(II) from water, Acta Chim. Slov. 62 (2015) 111–121, https://doi.org/10.17344/acsi.2014.787.
[108] F.N. Memon, H.F. Ayyilidiz, H. Kara, S. Memon, A. Kenar, M.K. Leghari, M. Topkafa, S.T.H. Sherazi, N.A. Memon, F. Durmaz, I. Tarhan, Application of central composite design for the optimization of on-line solid phase extraction of Cu2+ by calix[4]arene bonded silica resin, Chemom. Intell. Lab. Syst. 146 (2015) 158–168, https://doi.org/10.1016/j.chemolab.2015.05.020.
[109] V.N. Losev, O.V. Buyko, A.K. Trofimchuk, O.N. Zuy, Silica sequentially modified with polyhexamethylene guanidine and Arsenazo I for preconcentration and ICP–OES determination of metals in natural waters, Microchem. J. 123 (2015) 84–89, https://doi.org/10.1016/j.microc.2015.05.022.
[110] M. Koorepazan Moftakhar, Z. Dousti, M.R. Yaftian, M. Ghorbanloo, Investigation of heavy metal ions adsorption behavior of silica-supported Schiff base ligands, Desalin. Water Treat. 57 (2016) 27396–27408, https://doi.org/10.1080/19443994.2016.1170638.
[111] Z. Zhu, Preparation and characterization of functionalized silica spheres for removal of Cu(II), Pb(II), Cr(II) and Cd(II) from aqueous solutions, RSC Adv. 5 (2015) 28624–28632, https://doi.org/10.1039/c4ra14985h.
[112] S. Tighadouini, S. Radi, M. El Massaoudi, M. Bacquet, M. Zaghiroui, Adsorption of Cu(II) onto novel silica gel-immobilized bithiophene tripodal receptor, J. Mater. Environ. Sci. 6 (2015) 1457–1468.
[113] S. Radi, S. Tighadouini, M. Bacquet, S. Degoutin, L. Janus, Y.N. Mabkhot, Fabrication and covalent modification of highly chelated hybrid material based on silica-bipyridine framework for efficient adsorption of heavy metals: isotherms, kinetics and thermodynamics studies, RSC Adv. 6 (2016) 82505–82514, https://doi.org/10.1039/c6ra14349k.
[114] Y. Ruiz-Morales, HOMO−LUMO gap as an index of molecular size and structure for polycyclic aromatic hydrocarbons (PAHs) and asphaltenes: a theoretical study. I, J. Phys. Chem. A 106 (2002) 11283–11308, https://doi.org/10.1021/jp021152e.
[115] J. Aihara, Reduced HOMO−LUMO gap as an index of kinetic stability for polycyclic aromatic hydrocarbons, J. Phys. Chem. A 103 (1999) 7487–7495, https://doi.org/10.1021/jp990092i.
[116] D.E. Manolopoulos, J.C. May, S.E. Down, Theoretical studies of the fullerenes: C34 to C70, Chem. Phys. Lett. 181 (1991) 105–111, https://doi.org/10.1016/0009-2614(91)90340-f.